AD-A169 706 A MODIFIED LIGHTLY DOPED DRAIN STRUCTURE FOR VLSI MOSFET'S(U) STANFORD UNIV CA INTEGRATED CIRCUITS LAB S BAMPI ET AL. 1986 MDA903-84-K-0062 1/1

UNCLASSIFIED F/G 9/1 NL

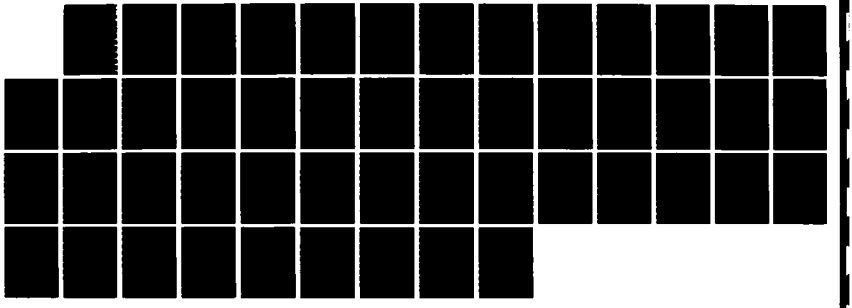

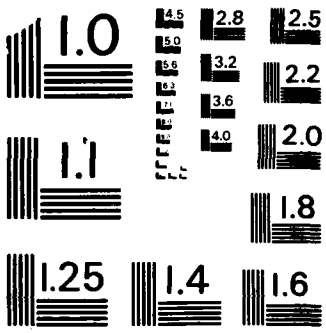

MICROCOPY RESOLUTION TEST CHART

NATIONAL BUREAU OF STANDARDS - 1963 - A

A MODIFIED LIGHTLY DOPED DRAIN STRUCTURE FOR VLSI MOSFET's

Sergio Bampi and James D. Plummer

Integrated Circuits Laboratory, Department of Electrical Engineering
Stanford University
Stanford, CA 94305

1986

Abstract

A new n-MOS LDD-like device structure (the J-MOS transistor) is proposed. Its design, simulation and fabrication are studied in this paper. N-channel MOSFET's with L_{eff} below 2μm suffer from high field effects that must be overcome to secure reliable 5 V operation. LDD structures alleviate these effects but their reliability is better than that of conventional MOSFET's only if the n^- regions have a peak doping density above $1 \times 10^{18}\text{cm}^{-3}$. To overcome this limitation and to allow constant voltage scaling for devices into the submicron regime, the J-MOS structure uses a series drain JFET to drop part of the supply voltage. Both 2-D device simulations and experimental results are presented to demonstrate the operation of this device and its potential for applications requiring reliable submicron device operation under maximum supply voltage. The major experimental findings are that the J-MOS structure can sustain 5 V operation even for submicron effective channel lengths. As has been the case with all LDD-like structures, improved device reliability has been achieved at the expense of some performance. However, the advantages of keeping 5 V operation in micron sized devices can outweight this performance loss.

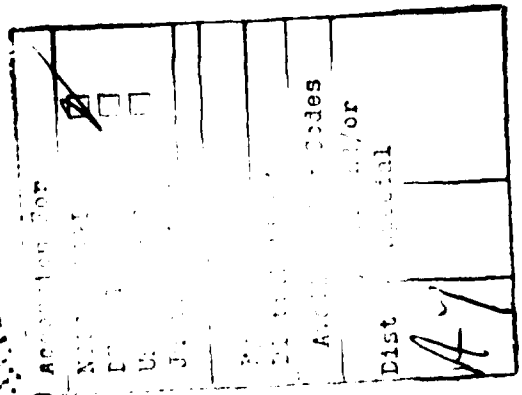

I. Introduction

Past experience in MOSFET scaling has shown that device design has proceeded under constraints other than those suggested by constant electric field scaling principles [1]. Alternative scaling approachs [2]–[4] have been used instead, which have allowed continued scaling under constant supply voltage. The shrinking of device dimensions while keeping supply voltage constant offers circuit and system performance advantages, in addition to compatibility with the established 5 V standard. This leads inevitably to higher electric fields inside the active regions of the transistors. Operation of micron and submicron MOSFET's in the presence of high field effects has called for inovation in their design so that acceptable device punch-through voltage and long-term device reliability are maintained as MOSFETs are scaled. In particular several LDD-like drain structures with the schematic cross sections of Fig. 1 have been studied and compared for use in VLSI circuits as substitutes for the conventional n^+ As-drain. Careful engineering of the drain region in n-channel devices is more important than in p-channel devices, because electrons in Si have a higher impact ionization rate, a lower energy barrier to injection into the oxide at the Si– SiO_2 interface, and saturate their drift velocity at smaller fields than holes. High field effects are then much more deleterious to n-channel device performance and reliability. Since device degradation [5]–[8] is related to heating of carriers as they traverse regions of field strength in excess of $100 KV/cm$, reducing electric fields at the drain end of the channel is crucial in n-channel devices. LDD designs for submicron p-channel devices have also been proposed [9], mostly for reasons of punch-through prevention.

In both the LDD–FET [10]–[20], and the graded S/D [21]–[27] – or double diffused drain (DDD) – n-channel structures of Fig. 1, the narrow, self–aligned n^- regions that are introduced between the channel and the self-aligned n^+ source-drain are designed to spread the high electric field at the drain pinch-off region into the n^- region. Other device structures using a non-self-aligned separate gate, buried channel, or lightly doped S/D have also been proposed [28]–[32]. The reduction and/or spreading of the peak E-field in self-aligned LDD-like structures normally results in an increased reliability insofar as hot electron induced instabilities are concerned. However, if the n^- surface doping (N_S) is

too light, i.e. $N_S < 10^{18}\text{cm}^{-3}$, the LDD-FET's can actually exhibit poorer reliability than conventional Arsenic-doped n^+ S/D transistors in addition to increased series resistance. This LDD related degradation has been shown to be caused by hot carrier injection into the sidewall oxide region [33]–[36] (process (2) in Fig. 2), which in turn leads to excessive series resistance and degradation rates faster than conventional designs [33,34]. At an optimum n^- doping level, process (1) of Fig. 2 should dominate as the longitudinal E-field peaks under the gate. The n^- resistive region of optimized LDD FETs spreads and reduces the peak value of the longitudinal electric field along the channel length, but the n^- region under the sidewall oxide must still remain undepleted for the aforementioned reliability reasons. While peak substrate current is usually reduced with a lighter n^- dose, characteristics of LDD devices can deteriorate more rapidly with n^- doses $< 10^{13}$ cm^{-2} [20,33,34,36,37]. Optimum LDD designs have been studied extensively, and for practical junction depths and S/D furnace anneal temperatures, the optimum N_S is $1-2.5\times10^{18}\text{cm}^{-3}$ [20,38], or, alternatively, the optimum n^- dose is $\simeq 1-2\times10^{13}$ cm^{-2} for "inside" LDD's of the type shown in Fig. 1 [36,39,40]. Other studies have proposed that better I_{SUB} and device degradation trade-off for "inside" LDD's occurs with either a moderately doped $(4-10\times10^{13}$ cm$^{-2})$ Phosphorous n^- region [41] or with a (shallow As)/(n^- P) profiled n^- region [42]. Optimum n^- implant doses were determined to be $\simeq 5-20\times10^{13}$ cm^{-2} for both "outside" LDD's (Fig. 1-d), which are a double-diffused type of structure self-aligned to the oxide spacer [43], and DDD MOSFET's (Fig. 1-b) [40,44]. A pseudo 2-D analytical model [45,46] would predict breakdown voltage improvements of less than 2 V and 1 V for DDD and "inside" LDD devices, respectively, in this practical, reliability-proven range of n^- doping levels.

II. JMOS Device Structure

In the search for reliable VLSI MOSFET's one should recognize the importance of both reducing high fields inside the device, and also keeping high fields as far away as possible from the most sensitive MOSFET region: the Si-SiO_2 interface, since most device instabilities are the result of damage to the gate oxide. In the JFET-MOSFET (JMOS) structure

that we have proposed [47], shown in Fig. 3, one seeks to keep the field peak away from the region under the gate, and at the same time force the electron current below the surface in the critical high field region near the drain, which should have the effect of minimizing hot carrier trapping in the gate or sidewall spacer SiO_2 regions. Other authors have also shown that LDD's can perform even more reliably by diverting the channel current away from the SiO_2 interface in the high field drain region. Techniques proposed to accomplish this include either a buried channel device with a lightly doped drain [48] or a retrogade n^- profile for the LDD region [49]. Other MOSFET device structures have been proposed, like the buried drain D-MOSFET [50], for which the reliability potential in VLSI has not yet been assessed. By construction the JMOS structure avoids the reliability problems found in lighter doped LDD devices associated with carrier injection into the sidewall oxide. Once gate oxide reliability is assured, one is allowed an increase in power supply or a reduction in MOSFET channel length at a given voltage to achieve a performance enhancement. The proposed structure in Fig. 3 has a short channel JFET at the drain end. The JFET physically occurs because of the presence of a p^+ region acting as the JFET gate above the n^- drain region (Fig. 3). The p^+ implant connects electrically to the substrate by overlapping the channel stop implant in the transverse direction. The circuit model for such device is shown in Fig. 4. The JFET under the sidewall oxide is fully merged into the MOSFET structure and does not require extra silicon area. It does require a minimum of one extra mask in the process.

III. Device Simulation

The JMOS circuit model of Fig. 4 was simulated using SPICE and the transfer function V_{D_i} vs. V_D is plotted in Fig. 5, where V_{T_J} is the JFET threshold voltage, V_{D_i} is the effective drain bias on the intrinsic MOSFET, and V_D is the externally-applied drain bias. The HPSPICE MOSFET level 3 and JFET model parameters used are listed in Table I. The simulation suggests that by appropriately choosing the JFET pinch-off voltage V_p, the device designer can limit the maximum drain bias across the surface channel MOSFET. Thus, the JMOS device provides a means of minimizing hot carrier problems imposed by

constant voltage scaling [7], since the series JFET can be designed to support part of the drain supply. When the MOSFET channel is conducting current, the inequality:

$$V_{D_i} < (|V_p| - \phi_{bi} - |V_{SUB}|) = V_{SUB} - V_{T_J} \quad . \tag{1}$$

holds, where V_p is the JFET region pinch-off voltage, and ϕ_{bi} is the p^+n^- junction built-in potential. In practical designs V_p, V_{T_J}, and V_{SUB} are ≤ 0. Limiting V_{D_i} could also be accomplished, of course, by reducing (most likely to 3 – 3.3 V) the supply voltage. However, this has important draw backs since such a reduction leads to compatibility problems, to smaller noise margins in circuits, and to reduced $(V_{GS} - V_T)$ MOSFET drive. Less gate drive often implies slower circuits. The presence of a series drain JFET in the JMOS device allows the full supply to be used on the V_D and V_G terminals, while the internal voltage of the reliability sensitive node – i.e. the MOSFET drain – is reduced. Conventionally designed micron sized n-MOSFET's in fact require drain biases of less than 3 V to saturate the channel current in the practical range $0 < (V_{GS} - V_T) < 5$ V, as shown in Fig. 6. This is simply the effect of saturation of the channel electron average velocity ($\langle v \rangle$). Submicron devices operating in this saturated velocity regime will have a drain saturation current given by

$$I_{DS_{sat}} = W \langle v \rangle C_{ox}(V_{GS} - V_T) \tag{2}$$

where $\langle v \rangle \simeq v_{sat}$ (the optical phonon scattering limited drift velocity for bulk transport). The drain JFET device, once it pinches off, limits the JMOS current approximately to its first order pinch-off limit I_p [51]

$$I_p = W I_{po} \left(1 - \left(\frac{\phi_{bi} + V_{D_i} + |V_{SUB}|}{|V_p|}\right)\right)^2 \tag{3}$$

$$I_{p_o} = \frac{|V_p|}{n \rho_s L_{sw}} \tag{4}$$

where n $(2 < n < 3)$ accounts for the non-uniform doping profile in the n^- JFET channel, $\rho_s(\Omega/\square)$ is the buried n^- sheet resistivity, L_{sw} is the sidewall spacer width – an approximate measure of the JFET effective electrical channel length – and $V_{D_i}(V_{GS})$ is the gate voltage dependent effective MOSFET drain or effective JFET source voltage, according to the

lumped circuit model proposed to describe the JMOS device. Eq. (3) neglects short JFET channel length effects which are more important when the n^- doping is lighter. The I_{po} value in $Amps/\mu m$ width depends on the technology design of the vertical impurity profile of the drain-JFET, as well as the sidewall spacer width.

The J-MOS device was simulated by the PISCES 2-D program [52,53] coupled to impurity profiles simulated in 1-D by SUPREM-III [54]. 2-D device simulations have been widely used as useful tools to guide and better understand the design of LDD devices [55]. Fig.7 shows the equipotential contours for the JMOS device under a bias condition in which the JFET under the sidewall oxide is in its linear region of operation. In this mode, the n^- region behaves as a series pinched resistor, or as a buried LDD structure. For the bias condition of Fig. 8, however, the saturation properties of the drain JFET are illustrated. For those biases in which the JFET is ON and pinched off, i.e.

$$(V_{DS} - V_{SUB}) \geq |V_{T_J}| \tag{5}$$

the saturated JFET limits the current in the device to the value of $I_p(V_{GS})$ given by Eq. (3). For the simulated device of Fig. 8 $V_{T_J} = -1.6\,\text{V}$, $V_{DS} = 5\,\text{V}$, $V_{SUB} = 0\,\text{V}$. The JFET pinch-off region then supports most of the 5 V drain bias on this particular JMOS design, while the surface channel MOSFET supports less than 1 V. As suggested by the simulated field pattern under the SiO_2/Si interface, and as we shall demonstrate experimentally, this will result in a large reduction in impact ionization under the MOSFET gate. The electron and net donor densities, and the electrostatic potential along the JMOS interface $A - A'$ are shown in Fig. 9-a and Fig. 9-b, respectively, for $V_{GS} = 1\,\text{V}$, $V_{DS} = 5\,\text{V}$, $V_{SUB} = -1\,\text{V}$. The peak longitudinal E–field at the gate SiO_2/Si interface is kept below 5×10^4 V/cm, which is one order of magnitude smaller than typical peak fields at the drain-end of pinched off conventional MOSFETs [56]–[58].

PISCES simulated I-V characteristics are shown in Fig. 10 for the device of Fig. 8. In this JMOS device the onset of saturation is independent of V_{GS} since the drain-JFET pinches off at the drain voltages for which Eq. (5) is an equality . In this case the JFET operates as a current-limiting device fully merged into the LDD region. The PISCES simulated transfer function (I_p/W) vs. V_{GS} is shown in Fig. 11, where I_p is the pinch-off

current of Eq. (3). A JFET short channel effect is responsible for the output conductance in Fig. 10 and the variation of $I_p(V_{GS})$ with V_{DS} in Fig. 11. This effect is quite easily seen in Fig. 8 as the drain field encroaches under the entire length of the p^+ JFET gate. Fig. 12 shows the same device under bias conditions that turn the JMOSFET off through the application of substrate bias, while the MOSFET surface is strongly inverted. In the case illustrated, V_{GS}=V_{DS}= 5V and $(V_{SUB} - V_{D_i}) \leq V_{T_J}$, i.e. the drain-JFET region is OFF and the MOSFET is ON. Thus, it is possible to turn off all JMOSFET's on a chip through appropriate substrate bias.

These device simulations have demonstrated the basic operation of the device. A variety of such simulations were used to suggest structural variations to optimize device performance. Control over the encroachment of high fields under the gate of the MOSFET can be achieved through proper design of the LDD region by adjusting the pinch-off voltage of the JFET region, V_p, to maximize device current drive while keeping short channel effects, and hot carrier injection into the gate oxide under tolerable limits.

IV. Device Fabrication

The fabrication process used is a standard 2μm n-MOS process using LOCOS isolation, a 400 Å gate oxide, and n^+ polysilicon gates. The starting material was $\langle 100 \rangle$, 20$-$25Ω-cm, boron doped silicon. A 900 Å Si_3N_4 on 400 Å SiO_2 mask was used during the local oxidation. The boron field implant dose was 1.5×10^{13}cm^2 at 120KeV. The field oxidation was done in steam at 1000°C/200 min.

Both conventional n-MOS devices and LDD n-MOS devices with 5 different variations in the source-drain regions were fabricated side by side, to test experimentally the JMOS device alongside the other better known LDD-MOSFET's. The major JMOS fabrication steps are shown in Fig. 13. By suitable combinations of the masked implants, all drain structures, including symmetrical JMOS and larger geometry JFET's, were fabricated side by side on the same chip. The asymmetric JMOS structure of Fig. 3 can be fabricated with only one extra masking step in addition to the conventional NMOS process if one

were to choose an LDD-type source structure and a drain JFET structure. Lightly doped source structures should either be doped above $5 \times 10^{18}\text{cm}^{-3}$ or be avoided altogether if transconductance reduction due to series source resistance [59]–[62] is to be kept low. Lighter doping levels are necessary on the drain, however, if one seeks to reduce the drain high field problem. In this work, 3 different n^- Phosphorous implant doses were used. Simulated surface concentrations for the n^- region were $8 \times 10^{17}\text{cm}^{-3}$ for a low V_p JFET, $2 \times 10^{18}\text{cm}^{-3}$, and $3 \times 10^{18}\text{cm}^{-3}$ for higher V_p JFETs, after a 1050°C, 60 min. drive-in of the Phosphorous implant. A shallow 100 KeV p^+ BF_2 implant followed to form the substrate-connected JFET gate on the JMOS devices. The 1050°C anneal assured sufficient lateral diffusion of the n^- implant to guarantee merging of the surface MOSFET channel and the JFET channel after the p^+ and n^+ implant anneals that followed. LDD region definition was done with a conventional sidewall spacer technology [63]-[64] by depositing 8,000 Å LPCVD oxide, followed by a 900°C/30 min. oxide densification, and oxide plasma etch. Final sidewall oxide spacer widths of 4,100 to 4,600 Å were obtained. Subsequently, conventional n^+ As S/D implant and a 900°C/30 min. anneal followed. SUPREM-III simulated profiles after all anneals for the high V_p and low V_p JFET designs, as well as for the n^+ As drain profile are shown in Fig. 14. Final MOSFET channel region boron surface concentration was $1.3 \times 10^{16}\text{cm}^{-3}$. Table II summarizes the relevant parameters for the two JMOS designs to be mentioned.

V. Experimental Results

A. I–V Characteristics

Fig. 15 shows the $\log(I_{DS}) - V_{GS}$ characteristics for the low–V_p JMOS device at $V_{DS} = 0.1$ V, in which both the JFET subthreshold and the MOSFET subthreshold regimes are illustrated. The drain current exhibits the usual exponential turn-on [65] in the MOSFET subthreshold regime. However, due to the drain JFET gating action, the drain current can be turned-off by setting $V_{SUB} < V_{T_J}$. For this low-V_p design $V_{T_J} = -(|V_p| - \phi_{bi}) = -0.8$ V. The long channel, zero backgate bias MOSFET threshold voltage is 0.32 V, as extracted by

the TECAP2 [66] fitting of the conventional device linear region $I_{DS} - V_{GS}$ characteristics at several substrate biases. Fully extracted conventional MOSFET parameters are shown in Table I.

A $(\frac{W}{L}) = (\frac{50}{2})$ JMOS device is compared to a conventional MOSFET of the same drawn gate length in Fig. 16. The JMOS effective channel lenght is $\approx 0.2\mu m$ shorter than its conventional counterpart on the same chip. At large V_{GS} the value of I_p given by Eq. (3) saturates to a value $I_{p_{max}}$ experimentally determined for devices with $L_{gate} = 2\mu m$. This saturated value of the JMOS I_{DS} for $V_{SUB} = 0V$, V_{GS}= V_{DS}=5 V is $I_p = 24\mu A/\mu m$, and is practically independent of MOSFET intrinsic channel length or polysilicon gate bias, so that the JFET acts as a current limiter in the device structure. This value compares reasonably well with the simulated value $I_{DS_{sat}} = 37\mu A/\mu m$, for a narrower sidewall spacer, and hence a shorter JFET length. The degree of current limiting by the JFET in this low-V_p design is more than what would be desired in an actual VLSI application but its characteristics are shown here to illustrate the JFET action as the two active devices are merged.

The I_{DS} - V_{DS} characteristics of JMOSFET's with higher V_p are compared to their conventional counterparts on the same chip in Figs. 17-18. These JMOSFET's have $I_{p_{max}}$ = 200 and 320 $\mu A/\mu m$ width, respectively. $I_{p_{max}}$ for the high-V_p design of Fig. 18 is larger than the 5 V current drive capability of our conventional enhancement n-MOS devices built with a 400 Å gate oxide, 2 μm technology. Hence, for large V_{DS} bias, short channel MOSFET, the JMOSFET saturation current limit is given by velocity saturation of the MOSFET inversion carriers, according to Eq. (2). In the high-V_p case, as shown in Fig. 18, the $I_{DS_{sat}}$ values are the same for both conventional and JMOSFET devices. In this case the operation of the drain-JFET is in its linear region, and the device acts as a simple buried LDD. This has the effect of increasing the linear region ON resistance of the JMOSFET. Drain series resistance for this case was extracted to be $10K\Omega - \mu m$ in excess of the conventional transistor series resistance, by using the measurement procedure of [67]. Based on measured sheet resistivity data for large geometry n^- pinched resistors, one concludes that the n^- buried LDD contribution to the series drain resistance does

not account for such series resistance increase. We believe that a sizable contribution to this ON resistance of the high V_p JMOSFET comes from the contact resistance of the Al(1%Si) metallization to the n^+ drain diffused layer which is compensated by the high dose (2.2×10^{14} cm^{-2}) p^+ JFET gate implant. Further improvements of this device structure are necessary to address two detrimental effects of including a shallow p^+ implant into the drain n^- region: first, the low breakdown voltage of the p^+ substrate/n^+drain junction; second, increased ON resistance due to impurity compensation of the surface n^- region; and third, the effect of the compensated p^+ layer on the contact resistance of the metal to n^+ region. These limitations can be overcome by more optimum design of the doping profiles in the drain region.

The 1050°C n^- drive-in step results in a fairly deep n^- junction in the high-V_p case, $\approx 0.7\mu m$ according to the simulation results in Fig. 14. Also, considerable diffusion of the channel implants for V_T adjustment and punchthrough suppression occurs. Scaling suggests that the S/D junction depths should be kept as shallow as technologically feasible. A JMOS device optimized for technologies with $L_{eff} < 1\mu m$ would have to use shallower junctions. The threshold voltage shift in the short channel regime should in turn be controlled by an appropriate choice of t_{ox} and punchtrough suppression implant dose. For the technology choices in this experiment, all devices had a linear region short-channel V_T shift of less than $100mV$ down to $L_{eff} = 1.25\mu m$ as shown in Fig. 19 for conventional (•), high-V_p (o), and graded S/D ($\triangle$) devices. The V_T measurement used for Fig. 19 assumes that the threshold voltage is given by the linear region (V_{DS}=0.1 V) extrapolation of the $I_{DS} - V_{GS}$ curves at the maximum value of transconductance $g_m = dI_{DS}/dV_{GS}$.

B. Substrate Current

In Fig. 20 the $\log(I_{SUB})$ vs. V_{GS} characteristics of both a conventional and a low-V_p JMOSFET (same device as Fig. 16) are compared for devices with the same drawn $(\frac{W}{L}) = (\frac{50}{1.5})$. The usual substrate current characteristics [68] are observed for the conventional MOSFET. Its bell-like shape indicates that the substrate current is mostly due to holes generated by impact ionization ocurring as carriers traverse the high field region under the gate in the

drain end of the device. The JMOSFET substrate current is mostly independent of gate voltage, it is not triggered by channel current, and it is more than 2 orders of magnitude lower than the peak value of the conventional device I_{SUB}. Except for the bias regime in which the conventional MOSFET is well into its linear mode of operation ($V_{GS}>V_{DS}$), i.e. the inversion layer extends from source to drain n^+ regions and decreases the longitudinal field strength in the drain end of the channel, the JMOS I_{SUB} is less than the conventional MOSFET impact ionization substrate current.

Drain diodes built on the same chip with different area/perimeter ratio confirmed that the JMOS substrate current shown in Fig. 20 is mostly p^+/n^+ sidewall diode leakage. This Zener-like drain–substrate leakage is fairly independent of channel current, hence independent of polysilicon gate length and MOSFET gate bias, and it scales with device width to a typical room temperature value of $\sim 300\,\mathrm{pA}/\mu\mathrm{m}$ at $V_{D-SUB} = 5\,\mathrm{V}$. In JMOS designs with higher n^- and p^+ doping densities, the Zener leakage under the same conditions can increase by orders of magnitude when tunneling becomes important, to a typical maximum of $\sim 500\,\mathrm{nA}/\mu\mathrm{m}$ when both sides of the sidewall junction were degenerately doped. High sensitivity to p^+ doping levels are expected for shallow $n^+(\mathrm{As})/p^+(\mathrm{Boron})$ junctions with p^+-doping levels above $10^{18}\mathrm{cm}^{-3}$ [69]. This suggests that an optimum JMOS design must pay careful attention to the p^+ doping profile in particular, if substrate current is to be minimized.

C. Gate Current

Very sensitive gate current measurements were done at the wafer level utilizing a floating gate induced drain current relaxation technique demonstrated in [70]. Resolution below $10^{-16}A$ was possible with this technique.

Gate current comparisons presented herein are for devices built side by side on the same chip, since small structural or doping variations can lead to invalid comparisons. Fig. 21 compares the gate current measured as a function of V_{GS} for a conventional, and for the low-V_p JMOSFET of Fig. 16 on the same chip. The former presents the characteristic bell-shaped peak that has been attributed to lucky channel hot carriers (CHE) [7,71], while the

JMOSFET gate current is below the noise level in the measuring apparatus. This extreme reduction of the gate current in the low-V_p JMOS device can be attributed to the reduction of the internal drain voltage V_{D_i} on the MOSFET due to the presence of the series JFET, even though the external V_{DS} is 7 V in this measurement. Fig. 21 also presents the gate current of the graded S/D device on the same chip, which gives an indication of impact ionization reduction due to drain profile grading alone. The reduction of the JMOSFET gate current is clearly due to a reduction of V_{D_i}, in addition to junction grading. This is consistent with the I-V characteristics of Fig. 16 and the substrate current characteristics of Fig. 20 which indicated that the JFET drain supported most of the drain bias and that impact ionization was negligible under the gate of the low-V_p JMOSFET, respectively.

Fig. 22 presents the gate current comparison for devices on the same chip of a high-V_p wafer, measured at V_{DS}= 6 V. Effective channel lengths are 1.25μm for the conventional MOSFET, and 1.0μm for the JMOSFET. In the CHE I_G peak (at $V_{GS} \simeq V_{DS}$) the reduction provided by the high-V_p JMOS is relatively small. At lower gate voltages, however, where impact ionization is more intense in conventional devices there is about one order of magnitude reduction in I_G measured in the JMOS structure. It is clear from Figures 21 and 22 that as the JFET pinch off voltage is reduced, the JFET increasingly limits the overall device current but also increasingly improves the gate current due to hot carriers.

D. Speed Performance

Ring oscillators with Fan-In=Fan-Out=1 were built to benchmark on the same chip the speed performance of the two JMOSFET device designs against conventional designs. The 21 inverter stages were of the n-channel enhancement / depletion type. Depletion and enhancement mode JMOSFET's were used in the JMOS inverter stages. All ring oscillators had the same drawn geometries: (12/3 drivers, 8/8 loads). Fig. 23 shows the oscillation period as a function of the supply voltage for two wafers. The speed performance of the low-V_p design (dashed line) is much degraded as compared to the conventional device speed ($\square$). This performance degradation is expected since the drive capability of the JMOS inverter stage is severely limited by the low-V_p drain JFET as shown in Fig. 16.

The high-V_p JMOS ring oscillator had a speed (solid line) comparable to the conventional design on the same chip (o). The slight speed-up for this JMOSFET design is solely attributable to the smaller L_{eff} of the transistors, ($\approx 0.25\mu m$ shorter), and it is within the wafer to wafer variation of the speed performance of the conventional devices. Usually in E/D circuits the average pull-up output current increases sublinearly with supply voltage. For this reason, the larger logic swing at larger supply voltages results in a slow down of the ring oscillator speed as V_{DD} increases, as shown in Fig. 23.

The introduction of the p^+ region in the JMOSFET drain has the positive effect of reducing the gate to n^+drain feedback capacitance (C_{GD}) at the expense of increasing both drain to substrate junction capacitance (C_{DSUB}) and gate to p^+ overlap/fringing capacitance (C_{GSUB}).

VI. Discussion

The JMOS structures studied have demonstrated the basic advantages of this device design. First, the maximum effective MOSFET drain bias can be set by device design, independently of the maximum externally applied drain and gate bias which can be set at effectively higher voltages. This property is advantageous in view of the pressing need for voltage reduction in conventional submicron MOSFET's brought on by hot carrier effects. Second, the JMOSFET lightly doped drain region can be engineered without the usual reliability constraint imposed on conventional LDDFET's due to hot carrier injection under the sidewall; reliable LDDFET's required $N_S > 10^{18}\text{cm}^{-3}$ in the n^- region, while the buried n^- region in the JMOSFET can be more lightly doped to meet the designer's choice for JFET V_p. Third, the advantages in channel longitudinal field reduction due to drain junction grading that are common to all LDD-like structures previously studied, are also present in the JMOSFET with the additional advantage of having the channel current driven away from the SiO_2 interface in the high-field drain region. All three features combined allow further minimization of charge injection, trapping, and instabilities associated with the gate oxide. Based on the proven correlation between gate and substrate

currents and device reliability found in both conventional and LDD-like devices, we expect submicron JMOSFET's to have good endurance under hot carrier stress.

Our implementations of the JMOSFET have pointed to areas that merit further improvement. First, the breakdown voltage of the sidewall n^+ p^+ junction at 6.5 V and the associated junction leakage seen at 5 V render the drain-to-substrate leakage unacceptable for dynamic circuit applications. The use of a phosphorous n^+ region self-aligned to the sidewall oxide or a slight ($\approx 0.2\mu m$) anisotropic silicon etch-back prior to arsenic n^+ implant in order to grade or eliminate the n^+ p^+ sidewall junction are possible technology implementations that can overcome this shortcoming. Second, a symmetrical JMOSFET suffers from a further effective transconductance decrease due to an increase in series source resistance (R_S), since

$$g_{m_{sym}} = \frac{g_{m_J}}{1 + g_{m_J} R_S} \tag{6}$$

where g_{m_J} and $g_{m_{sym}}$ are the JMOSFET and symmetrical JMOSFET effective transconductances respectively. This likely means that an extra mask must be used to eliminate the p^+ region on the source side. Third, process complexity and control are relevant issues in the comparison of the JMOSFET and more conventional designs. The presence of a self-aligned active device under the oxide spacer that controls the current drive of the JMOSFET, makes oxide spacer process control even more necessary. The addition of at least one extra masking step with worst-case alignment tolerance of $L_{gate}/2$ is one additional draw back of the JMOSFET in its asymmetric implementation.

VII. Conclusions

The JMOSFET, a modified LDD device structure has been proposed, designed, modeled and experimentally demonstrated. It provides device designers with tradeoffs in performance somewhat different than LDD devices previously reported. The JMOS device can be optimized for a given technology choice of minimum effective channel length, oxide thickness, and supply voltage. It overcomes some of the reliability problems of LDD devices with peak doping densities below $1 \times 10^{18}\text{cm}^{-3}$ related to injection into the sidewall oxide.

By keeping the longitudinal E-field peak away from the SiO_2/Si interface, the JMOSFET structure minimizes hot carrier injection into the oxide – as made evident through gate and substrate current characteristics – and should minize also the reliability problems associated with that injection. Our results suggest that with proper optimization of the drain JFET this new structure can perform well in VLSI applications, while maintaining its hot carrier resistant properties in submicron 5 V supply circuits. As has been the case with all LDD-like structures, improved device reliability has been achieved at some expense in performance. However, the advantages of keeping the 5 V operation in micron sized devices can outweight this performance loss.

Acknowledgements

S. Bampi gratefully ackowledges a scholarship provided by CNPq - Brazilian Research Council, and the students and staff of the Integrated Circuits Laboratory for their support in simulation, wafer fabrication and testing. This work was partially supported by DARPA under contract MDA903-84-K-0062.

References

[1] Robert H. Dennard, Fritz H. Gaensslen, Hwa-Nien Yu, V. Leo Rideout, Ernest Bassous, and Andre R. LeBlanc, "Design of Ion-Implanted MOSFET's with Very Small Physical Dimensions", *IEEE J. Solid-State Circuits*, vol. **SC-9**, pp. 256-267, October 1974.

[2] J. R. Brews, W. Fichtner, E. H. Nicollian, and S. M. Sze, "Generalized Guide for MOSFET Miniaturization", *IEEE Electron Device Lett.*,vol. **EDL-1**, pp. 2-4, January 1980.

[3] P. Chaterjee, W. Hunter, T. Holloway, and Y. Lin, "The Impact of Scaling Laws on the Choice of n-Channel or p-Channel for MOS VLSI", *IEEE Electron Device Lett.*,vol. **EDL-1**, pp. 220-223, Oct. 1980.

[4] Giorgio Baccarani, Matthew R. Wordeman, and Robert H. Dennard, "Generalized Scaling Theory and Its Application to a 1/4 Micrometer MOSFET Design", *IEEE Trans. Electron Devices*, vol. **ED-31**, pp. 452-462, April 1984.

[5] S. A. Abbas, and R. C. Dockerty, "Hot-Carrier Instability in IGFET's", *Applied Phys. Lett.*, vol. **27**, pp. 147-148, August 1975.

[6] P. E. Cottrell, R. R. Troutman, and T. H. Ning, "Hot-Electron Emission in n-Channel IGFET's", *IEEE J. Solid-State Circuits*, vol. **SC-14**, pp. 442-455, April 1979.

[7] T. H. Ning, P. W. Cook, R. H. Dennard, C. M. Osburn, S.E. Schuster, and H. N. Yu, " 1 μm MOSFET VLSI Technology: Part IV – Hot-Electron Design Constraints ", *IEEE Trans. Electron Devices*, vol. **ED-26**, pp. 346-352, April 1979.

[8] R. B. Fair, and R. C. Sun, "Threshold-Voltage Instability in MOSFET's due to Channel Hot-Hole Emission", *IEEE Trans. Electron Devices*, vol. **ED-28**, pp. 83-93, January 1981.

[9] Adele E. Schmitz, and John Y. Chen, "Design, Modeling, and Fabrication of Subhalf-Micrometer CMOS Transistors", *IEEE Trans. Electron Devices*, vol. **ED-33**, pp. 148-153, Jan. 1986.

[10] K. Saito, T. Morase, S. Sato, U. Harada, "A New Short Channel MOSFET with Lightly Doped Drain", (in Japanese) *Denshi Tsushin Rengo Taikai*, pp. 220, Apr. 1978.

[11] K. Ohta, K. Yamada, K. Shimizu, and Yasuo Tarui, "A Quadruply Self-Aligned MOS (QSA MOS): A New Short Channel High Speed High Density MOSFET for VLSI", *IEEE Int. Electron Devices Meet., Dig. Tech. Papers*, pp. 581-584, 1979.

[12] K. Ohta, K. Yamada, M. Saitoh, K. Shimizu, and Yasuo Tarui, "Quadruply Self-Aligned MOS (QSA MOS) – A New Short-Channel High-Speed High-Density MOSFET for VLSI", *IEEE Trans. Electron Devices*, vol. **ED-27**, pp. 1352-1358, Aug. 1980.

[13] S. Ogura, P.J. Tsang, W.W. Walker, D.L. Critchlow, and J.F. Shepard, "Design Characteristics of the Ligthly Doped Drain–Source (LDD) Insulated Gate Field-Effect Transistor", *IEEE Trans. Electron Devices*, vol. **ED-27**, pp. 1359-1367, Aug. 1980.

[14] S. Ogura, P.J. Tsang, W.W. Walker, D.L. Critchlow, and J.F. Shepard, "Elimination of Hot Electron Gate Current by the Lightly Doped Drain-Source Structure", *IEEE Int. Electron Devices Meet., Dig. Tech. Papers*, pp. 651, 1981.

[15] S. Hsia, R. Fatemi, T.C. Teng, S. Deornellas, and S.C. Sun, "Polysilicon Oxidation Self-Aligned MOS (POSA MOS) – A New Self-Aligned Double Source/Drain Ion Implantation Technique for VLSI", *IEEE Electron Device Lett.*,vol. **EDL-3**, pp. 40-42, February 1982.

[16] Paul J.Tsang, Seiki Ogura, W. Walker, J. Shepard, and D. Critchlow, "Fabrication of High-Performance LDDFET's with Oxide Sidewall-Spacer Technology", *IEEE Trans. Electron Devices*, vol. **ED-29**, pp. 590-595, April 1982.

[17] E. Takeda, H. Kume, T. Toyabe, and S. Asai, "Submicrometer MOSFET Structure for Minimizing Hot-Carrier Generation", *IEEE Trans. Electron Devices*, vol. **ED-29**, pp. 611-618, Apr. 1982.

[18] Seiki Ogura, Christopher F. Codella, Nivo Rovedo, Joseph F. Shepard, and Jacob Riseman, "A Half Micron MOSFET Using Double Implanted LDD", *IEEE Int. Electron Devices Meet., Dig. Tech. Papers*, pp. 718-721, 1982.

[19] S. Ratham, H. Bahramian, D. Laurent, and Yu-Pin Han, "An Optimized 0.5 Micron LDD Transistor", *IEEE Int. Electron Devices Meet., Dig. Tech. Papers*, pp. 237-241, 1983.

[20] Y. Matsumoto, T. Higuchi, S. Sawada, S. Shinozaki and O. Ozawa, "Optimized and Reliable LDD Structure for 1 μm NMOSFET Based on Substrate Current Analysis", *IEEE Int. Electron Devices Meet., Dig. Tech. Papers*, pp. 392-395, 1983.

[21] H. Sunami, K. Shimohigashi, and N. Hashimoto, "Characteristics of a Buried-channel Graded Drain with Punchthrough Stopper (BGP) MOS Device", *IEEE Trans. Electron Devices*, vol. **ED-29**, Apr. 1982.

[22] S. Satoh, Y. Ohbayashi, K. Mizuguchi, M. Yoneda, and H. Abe, " Self-aligned Graded-Drain Structure for Short Channel MOS Transistor", *Symp. VLSI Technol. Digest Tech. Papers*, pp. 38, 1982.

[23] M.L. Chen, B.C. Leung, A.G.F. Dingwall, and B. Lalevic, " Self-Registered Gradually Doped Source Drain Extension Short Channel CMOS/SOS Devices", *IEEE Electron Device Lett.*,vol. **EDL-3**, pp. 387-390, Dec. 1982.

[24] E. Takeda, H. Kume, Y. Nakagome, T. Makino, A.Shimizu, and S. Asai, "An As-P(n^+/n^-) Double Diffused Drain MOSFET for VLSI's", *IEEE Trans. Electron Devices*, vol. **ED-30**, pp. 652-657, June 1983.; also E. Takeda, H. Kume, Y. Nakagome, and S. Asai, "An As-P(n^+/n^-) Double Diffused Drain MOSFET for VLSI's", *Symp. VLSI Technol. Digest Tech. Papers*, pp. 40, 1982.

[25] K. Balasubramanyam, M.J. Hargrove, H.I. Hanafi, M.S. Lin, D. Hoyniak, J. LaRue, and D.R. Thomas, "Characterization of As-P Double Diffused Drain Structure", *IEEE Int. Electron Devices Meet., Dig. Tech. Papers*, pp. 782-785, Dec. 1984.

[26] S. Aur, P. Yang, P. Pattnaik, and P.K. Chatterjee, "Modeling of Hot Carrier Effects for LDD MOSFETs", *Symp. VLSI Technol. Digest Tech. Papers*, pp. 112-113, 1985.

[27] Y. Tsunashima, T. Wada, *et al.*"Metal-Coated Lightly-Doped Drain (MLD) MOSFET's for Sub-micron VLSI's", *Symp. VLSI Technol. Digest Tech. Papers*, pp. 114-115, 1985.

[28] Ken Yamaguchi, Susumu Takahashi, and Hiroshi Kodera, "Theoretical Study of a Channel-Doped Separate Gate Si MOSFET (SG-MOSFET) by Two-Dimensional Computer Simulation", *IEEE Trans. Electron Devices*, vol. **ED-28**, pp. 117-120, January 1981.

[29] Ken Yamagushi and Susumu Takahashi, "Submicron Gate MOSFET's with Channel-Doped Separate Gate Structure (SG-MOSFET's)", *IEEE Trans. Electron Devices*, vol. **ED-28**, pp. 888-890, July 1981.

[30] R. E. Howard, L. D. Jackel *et al.*, "Buried Channel MOSFET's with Gate Lengths from 2.5μm to 700 Å", *IEEE Electron Device Lett.*,vol. **EDL-3**, pp. 322-324, October 1982.

[31] R. G. Swartz, R. E. Howard *et al.*, "700 Å Gate Lenght Buried Channel Silicon MOSFET's", *IEEE Int. Electron Devices Meet., Dig. Tech. Papers*, pp. 642-645, 1982.

[32] L. D. Jackel, R.G. Swartz *et al.*, "CASFET: A MOSFET-JFET Cascode Device with Ultralow Gate Capacitance", *IEEE Trans. Electron Devices*, vol. **ED-31**, pp. 1752-1757, December 1984.

[33] F.C. Hsu, and H.R. Grinolds, "Structure-Enhanced MOSFET Degradation Due to Hot-Electron Injection", *IEEE Electron Device Lett.*,vol. **EDL-5**, pp. 71-74, March 1984. – also "Structure-Dependent MOSFET Degradation Due to Hot-Electron Injection", *IEEE Int. Electron Devices Meet., Dig. Tech. Papers (Late News)*, pp. 742-744, 1983.

[34] F.-C. Hsu, and K.-Y. Chiu, " Evaluation of LDD MOSFET's Based on Hot-Electron-Induced Degradation", *IEEE Electron Device Lett.*,vol. **EDL-5**, pp. 162-165, May 1984.

[35] Y. Toyoshima, H. Nihira, M. Wada, and K. Kanzaki, "Mechanism of Hot Electron Induced Degradation in LDD NMOS-FET", *IEEE Int. Electron Devices Meet., Dig. Tech. Papers*, pp. 786-789, 1984.

[36] H. Katto, K. Okuyama, S. Meguro, R. Nagai, and S. Ikeda, "Hot Carrier Degradation Modes and Optimization of LDD MOSFETs", *IEEE Int. Electron Devices Meet., Dig. Tech. Papers*, pp. 774-777, 1984.

[37] Sunil N. Shabde, Fariborz Barman, and Anjan Bhattacharyya, "Channel-Length Dependence of Substrate Current Characteristic of LDD MOSFET's", *IEEE Trans. Electron Devices*, vol. **ED-32**, pp. 1885-1887, September 1985.

[38] C. Werner, R. Kuhnert, and L. Risch, "Optimization of Lightly Doped Drain MOSFETs Using a New Quasiballistic Simulation Tool", *IEEE Int. Electron Devices Meet., Dig. Tech. Papers*, pp. 770-773, 1984.

[39] Kueing-Long Chen, Steve Saller, and Rajiv Shah, "Some Methods to Reduce Hot Carrier Effects", *Symp. VLSI Technol. Digest Tech. Papers*, pp. 102-103, 1985.

[40] Hiroaki Mikoshiba, Tadahiko Horiuchi, and Kuniyuki Hamano, "Comparison of Drain Structures in n-Channel MOSFET's", *IEEE Trans. Electron Devices*, vol. **ED-33**, pp. 140-144, January 1986.

[41] Masaaki Kinugawa, Masakazu Kakumu, Shunji Yokogawa, and Kazuhiko Hashimoto, "Submicron MLDD NMOSFETs for 5 V Operation", *Symp. VLSI Technol. Digest Tech. Papers*, pp. 116-117, 1985.

[42] Y. Toyoshima, N. Nihira, and K. Kanzaki, "Profiled Lightly Doped Drain (PLDD) Structure for High Reliable NMOS-FETs", *Symp. VLSI Technol. Digest Tech. Papers*, pp. 118-119, 1985.

[43] David A. Baglee, Charvaka Duvvury, Michael C. Smayling, and Michael P. Duane, "Lightly Doped Drain Transistors for Advanced VLSI Circuits", *IEEE Trans. Electron Devices*, vol. **ED-32**, pp. 896-902, May 1985.

[44] M. Koyanagi, H. Kaneko, and S. Shimizu, "Optimum Design of n^+/n^- Double-Diffused Drain MOSFET to Reduce Hot-Carrier Emission", *IEEE Trans. Electron Devices*, vol. **ED-32**, pp. 562-570, March 1985.

[45] F. S. Lai, " An Analytic Model to Estimate the Avalanche Breakdown Voltage Improvement for LDD Devices", *Solid-State Electronics*, vol. **28**, pp. 959-965, October 1985.

[46] Fang-Shi J. Lai, and Jack Yuan-Chen Sun, " An Analytical One-Dimensional Model for Lightly Doped Drain (LDD) MOSFET Devices", *IEEE Trans. Electron Devices*, vol. **ED-32**, pp. 2803-2811, December 1985.

[47] S. Bampi and J. D. Plummer, "Modified LDD Device Structures for VLSI", *IEEE Int. Electron Devices Meet., Dig. Tech. Papers*, pp. 234-237, 1985.

[48] M. Nakahara, Y. Hiruta, T. Noguchi, M. Yoshida, K. Maeguchi, and K. Kanzaki, "Relief of Hot Carrier Constraint on Submicron CMOS Devices by Use of a Buried Channel Structure", *IEEE Int. Electron Devices Meet., Dig. Tech. Papers*, pp. 238-241, 1985.

[49] Hugh R. Grinolds, Masaaki Kinugawa, Masakazu Kakumu, "Reliability and Performance of Submicron LDD MOSFET's with Buried-As n^- Impurity Profiles", *IEEE Int. Electron Devices Meet., Dig. Tech. Papers*, pp. 246-249, 1985.

[50] W. Fichtner, J. A. Cooper, A. R. Tretola, D. Kahng, "A Novel Buried-Drain DMOSFET Structure", *IEEE Trans. Electron Devices*, vol. **ED-29**, pp. 1785-1791, Nov. 1982.; also "A Novel Buried Drain DMOSFET Structure", *IEEE Int. Electron Devices Meet., Dig. Tech. Papers*, pp. 363-366, 1981.

[51] S. M. Sze, "*Physics of Semiconductor Devices*", p.348 New York: Wiley-Interscience, 1969.

[52] Price, Craig H., "Two-Dimensional Numerical Simulation of Semiconductor Devices", *Stanford Electronics Laboratories Technical Report*, May 1982.

[53] M. R. Pinto, C. S. Rafferty, and R. W. Dutton, "PISCESII : Poisson and Continuity Equation Solver", *Stanford Electronics Laboratories Technical Report*, Sept. 1984.

[54] Charles P. Ho *et al.*, "SUPREM-III – A Program for Integrated Circuit Process Modeling and Simulation", *Stanford Electronics Laboratories Technical Report No. SEL84-001*, July 84.

[55] A. Schutz, and C. Werner, "State-of-the-Art of MOS Modelling", *IEEE Int. Electron Devices Meet., Dig. Tech. Papers*, pp. 766-769, 1984.

[56] Y. A. El-Mansy and A. R. Boothroyd, "A Simple Two-Dimensional Model for IGFET Operation in the Saturation Region", *IEEE Trans. Electron Devices*, vol. **ED-24**, pp. 254-262, March 1977.

[57] Chenming Hu, "Hot-Electron Effects in MOSFET's", *IEEE Int. Electron Devices Meet., Dig. Tech. Papers*, pp. 176-181, 1983.

[58] T.Y. Chan, P.K. Ko, and C. Hu, "Dependence of Channel Electric Field on Device Scaling", *IEEE Electron Device Lett.*,vol. **EDL-6**, pp. 551-553, October 1985.

[59] C. Duvvury, D.A. Baglee, M.C. Smayling, and M.P.Duane, "Series Resistance Modeling for Optimum Design of LDD Transistors", *IEEE Int. Electron Devices Meet., Dig. Tech. Papers*, pp. 388-391, 1983.

[60] Charvaka Duvvury *et al.*, "An Analytical Method for Determining Intrinsic Drain/Source Resistance of Lightly Doped Drain (LDD) Devices", *Solid-State Electronics*, vol. **27**, pp. 89-96, Jan. 1984.

[61] Steven E. Laux, "Accuracy of an Effective Channel Length/External Resistance Extraction Algorithm for MOSFET's", *IEEE Trans. Electron Devices*, vol. **ED-31**, pp. 1245-1251, Sept. 1984.

[62] B.J. Sheu, C. Hu, P.K. Ko, and F.C. Hsu; "Source-and-Drain Series Resistance of LDD MOSFET's", *IEEE Electron Device Lett.*,vol. **EDL-5**, pp. 365-367, Sept. 1984.

[63] P. J. Tsang, J.F. Shepard, J. Lechaton, and S. Ogura, "Characterization of sidewall-spacers Formed by Anisotropic RIE", *J. Electrochem. Soc.*, vol. **128**, pp. 238C, 1981. – also P.J. Tsang, J. F. Shepard, J. Lechaton, and S. Ogura, "Characterization of Sidewall-Spacers Formed by Anisotropic RIE", RNP553 ECS Spring Meeting Minneapolis, MN, 1981.

[64] P.J. Tsang, J.F. Shepard, S. Ogura, and J. Riseman, "Sidewall Spacer Technology", ECS Fall Meeting, Abstract 233 pp. 373-374, Oct. 1982.

[65] Richard M. Swanson, and J. D. Meindl, "Ion-Implanted Complementary MOS Transistors in Low-Voltage Circuits", *IEEE J. Solid-State Circuits*, vol. **SC-7**, April 1972.

[66] Hewlett-Packard Co., TECAP2 Reference Manual, *DA355* March 1984.

[67] Paul I. Suciu, and Ralph L. Johnston, "Experimental Derivation of the Source and Drain Resistance of MOS Transistors", *IEEE Trans. Electron Devices*, vol. **ED-27**, pp. 1846-1848, 1980.

[68] A. Henning, N. Chan, and J. Plummer, "Substrate Current in N-Channel and P-Channel MOSFETs Between 77 Kand 300 K: Characterization and Simulation", *IEEE Int. Electron Devices Meet., Dig. Tech. Papers*, pp. 573-576, 1985.

[69] J.M.C. Stork, and R.D. Isaac, "Bipolar Device Scaling Limits From Tunneling in Base-Emitter Junctions", *IEEE Int. Electron Devices Meet., Dig. Tech. Papers*, pp. 404-407, 1983.

[70] F. H. Gaensslen, and J. M. Aitken, "Sensitive Technique for Measuring Small MOS Gate Currents", *IEEE Electron Device Lett.*,vol. **EDL-1**, pp. 231-233, November 1980.

[71] Eiji Takeda, Norio Suzuki, and Takaaki Hagiwara, "Device Performance Degradation due to Hot-Carrier Injection at Energies Below the Si-SiO_2 Energy Barrier", *IEEE Int. Electron Devices Meet., Dig. Tech. Papers*, pp. 396-399, 1983.

TABLE I

MOSFET DEVICE PARAMETERS			
Name	*Symbol*	*Value*	*Unit*
Low field mobility	μ_o	665	$cm^2V^{-1}sec^{-1}$
Oxide thickness	t_{oz}	393	Å
Transconductance factor	K_P	58.5	μAV^{-2}
Threshold voltage	V_{T_O}	0.32	V
Effective substrate doping	N_{SUB}	9.1×10^{15}	cm^{-3}
Body factor	γ	0.515	$V^{-1/2}$
$(L_{mask} - L_{eff})/2$	L_D	0.25	μm
Gate field mobility factor	$\Theta\ (V_{NORM}^{-1})$	0.061	V^{-1}
Longitudinal field mob. factor	E_{TRA}	7.3×10^4	$V\ cm^{-1}$
Critical field	E_{CRIT}	1.7×10^4	$V\ cm^{-1}$
Saturated drain conductance	DE_{SAT}	7.9×10^9	$V\ cm^{-2}$
JFET DEVICE PARAMETERS			
Threshold voltage	V_{T_J}	$-1, -3, -5$ *	V
Transconductance factor	β	20, 40, 50 *	μAV^{-2}
Channel length modulation	λ	0.05	V^{-1}

* JFET1, JFET2, JFET 3

TABLE II

PROCESS PARAMETERS			
PARAMETER	*Low V_p Process*	*High V_p Process*	*Unit*
N^- Phosphorous Dose	2×10^{13}	7.5×10^{13}	cm^{-2}
Phosphorous surface conc. (N_S)	8×10^{17}	3×10^{18}	cm^{-3}
P^+ BF_2 Dose	6×10^{13}	2.2×10^{14}	cm^{-2}
N^- sheet resistance (ρ_s)	850	410	$\Omega/\square$
Pinched N^- ρ_s	5.8	1.2	$k\Omega/\square$
Oxide thickness (t_{oz})	400	400	Å
Sidewall width (L_{sw})	0.4	0.4	μm

Figure Captions

Fig. 1. Schematic cross-section of: (a) conventional (b) double diffused drain (c) "inside" LDD (d) "outside" LDD n-channel device structures.

Fig. 2. N-type LDD MOSFET device structure. Hot carrier injection occurs either (1) under the gate or (2) over the n^- depleted region under the sidewall oxide in case the light n^- dose allows for a non-overlapping drain depletion edge and gate electrode.

Fig. 3. The n-type JFET-MOSFET (JMOSFET) device structure.

Fig. 4. Equivalent circuit model for the JMOSFET device.

Fig. 5. Voltage transfer function from the externally applied JMOSFET drain bias (V_{DS}) and the voltage at the intrinsic drain of the surface channel MOSFET (V_{D_i}) for three different JFET designs.

Fig. 6. Saturation drain voltage dependence on $V_{GS} - V_T$ for a conventional n-channel MOSFET.

Fig. 7. PISCES simulated equipotential contours for the JMOSFET with $L_{eff} = 0.72\mu m$, $t_{ox} = 200\,\text{Å}$, $V_{T_J} = -1.6\,\text{V}$, V_{SUB}=0 V. Linear region bias of JFET. V_{DS}=0.1 V V_{GS}=1 V.

Fig. 8. PISCES simulated equipotential contours for the JMOSFET of Fig.7. JFET is pinched off at V_{DS}=V_{GS}=5 V.

Fig. 9. PISCES simulated variation of: a) Electron and (input-specified) Net Donor densities; b) Potential along Si/SiO2 interface (line $A - A'$). JMOS structure of Fig.7. $V_{SUB} = -1\,\text{V}$, $V_{DS} = 5\,\text{V}$, V_{GS}= 1 V.

Fig. 10. PISCES simulated $I_{DS} - V_{DS}$ for $V_{T_J} = -1.6\,\text{V}$. JMOSFET structure of Fig.7. $V_{SUB} = 0\,\text{V}$.

Fig. 11. Pinch-off current per unit channel width dependence on V_{GS}. PISCES simulated for the JMOSFET structure of Fig.7. $V_{SUB} = 0\,\text{V}$.

Fig. 12. Pisces simulated equipotential contours for the JMOSFET sctructure of Fig.7. V_{DS}=V_{GS}=5 V. MOSFET is ON and JFET is OFF at $V_{SUB} = -2\,\text{V}$.

Fig. 13. Process sequence for JMOS fabrication.

Fig. 14. SUPREM simulated impurity profiles for both JFET high-V_p and low-V_p designs.

Fig. 15. Measured subthreshold characteristics for the low-V_p JMOSFET. $(W/L) = (50/10)$, V_{DS}=0.1 V , V_{SUB} steps $\Delta V_{SUB} = -0.25\,V$ from 0 to $-1.75\,V$.

Fig. 16. Comparison of measured $I_{DS} - V_{DS}$ characteristics for the low-V_p JMOSFET and conventional device. Both devices have the same drawn $(W/L) = (50/2)$.

Fig. 17. Comparison of measured $I_{DS} - V_{DS}$ characteristics for a higher V_p JMOSFET and conventional device. Both devices have the same drawn $(W/L) = (50/2)$.

Fig. 18. Comparison of measured $I_{DS} - V_{DS}$ characteristics for the high-V_p JMOSFET and conventional device. Both devices have the same drawn $(W/L) = (50/2)$.

Fig. 19. Linear region threshold shift as a function of effective channel length. V_T extrapolation measurement at V_{DS}=100 mV.

Fig. 20. Substrate current vs. V_{GS} comparison for conventional (solid line) and low-V_p JMOS (dashed) at V_{DS}=3,4,5 V. Drawn $(W/L) = (50/1.5)$ for both devices. Low-V_p $L_{eff} = 0.8\mu m$, conv $L_{eff} = 1.0\mu m$.

Fig. 21. Gate current vs. V_{GS} comparison for conventional and low-V_p devices. Both have drawn $(W/L) = (50/2)$. Conv. $L_{eff} = 1.5\mu m$, JMOS $L_{eff} = 1.3\mu m$. V_{DS}=7 V, $V_{SUB} = 0$ V. Graded S/D device with $L_{eff} = 1.1\mu$ is also shown.

Fig. 22. Gate current vs. V_{GS} comparison for conventional and High-V_p devices. Both have drawn $(W/L) = (50/1.75)$. Conv. $L_{eff} = 1.2\mu m$, JMOS $L_{eff} = 1.0\mu m$. V_{DS}=6 V, $V_{SUB} = 0$ V.

Fig. 23. E/D ring-oscillator period of oscillation vs. supply voltage. Boxes (□ ■) indicate the low-V_p experiment. Circles (○ ●) indicate the high-V_p experiment

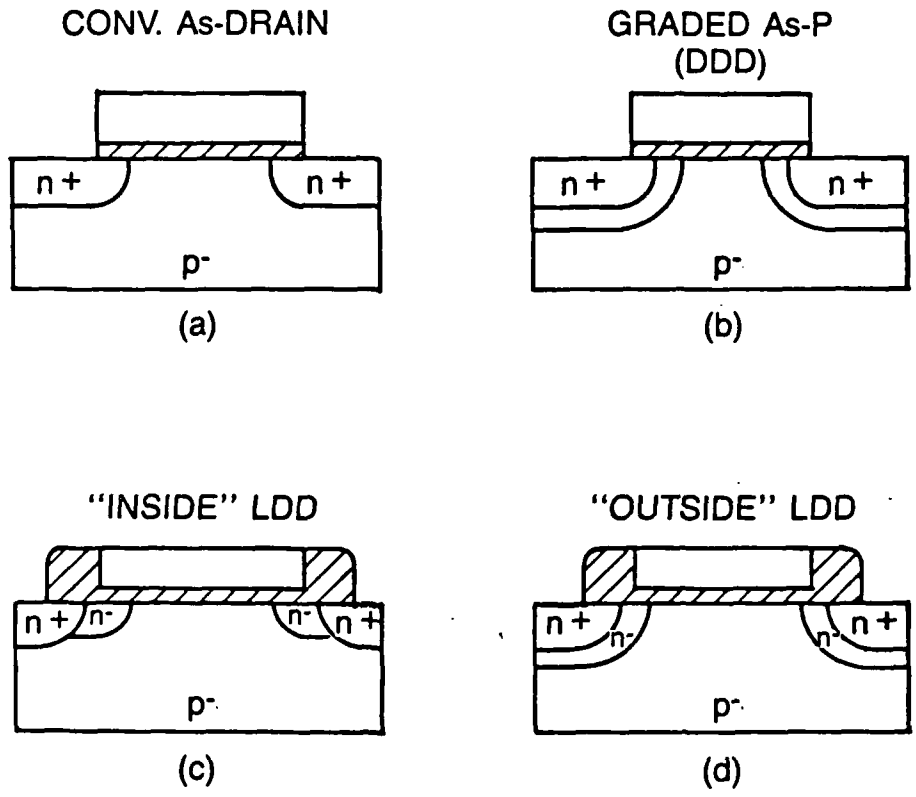

Fig. 1. Schematic cross-section of: (a) conventional (b) double diffused drain (c) "inside" LDD (d) "outside" LDD n-channel device structures.

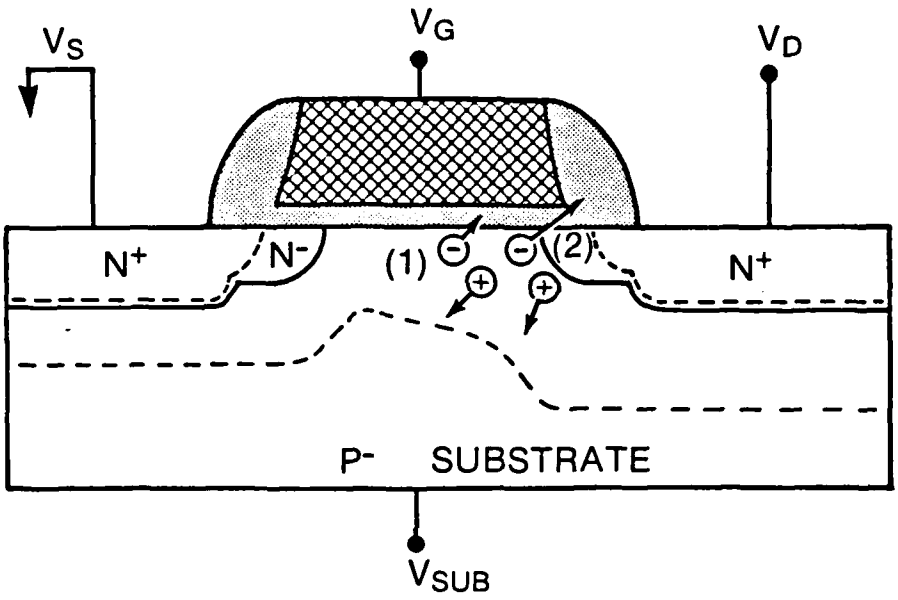

Fig. 2. N-type LDD MOSFET device structure. Hot carrier injection occurs either (1) under the gate or (2) over the n^- depleted region under the sidewall oxide in case the light n^- dose allows for a non-overlapping drain depletion edge and gate electrode.

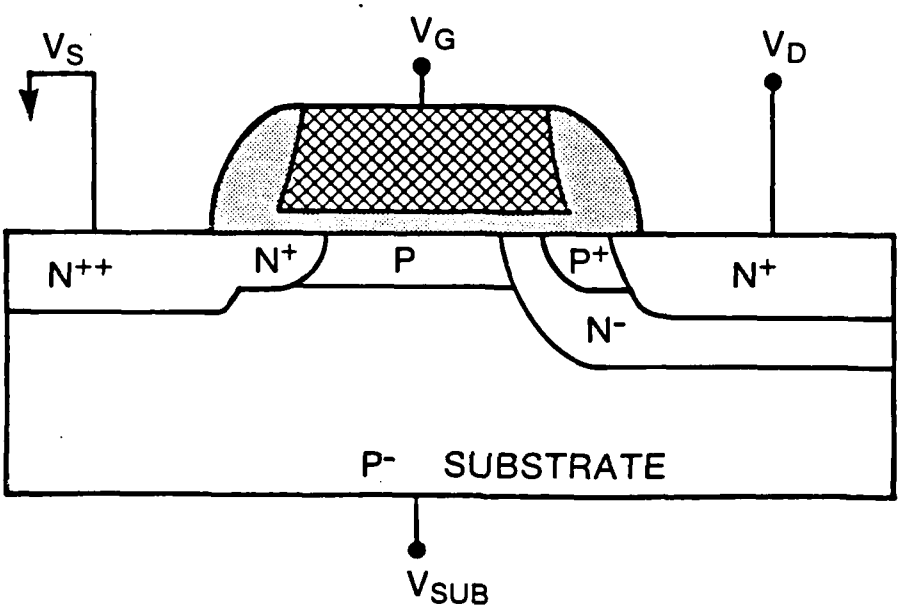

Fig. 3. The n-type JFET-MOSFET (JMOSFET) device structure.

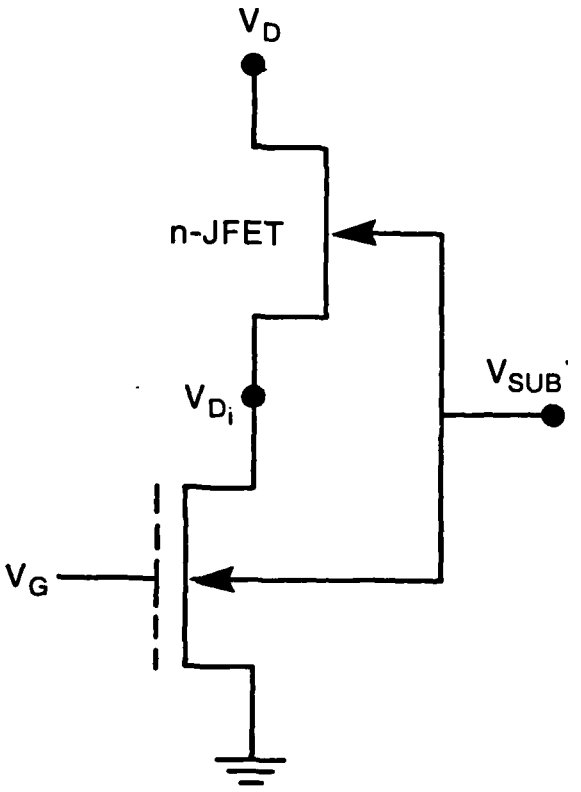

Fig. 4. Equivalent circuit model for the JMOSFET device.

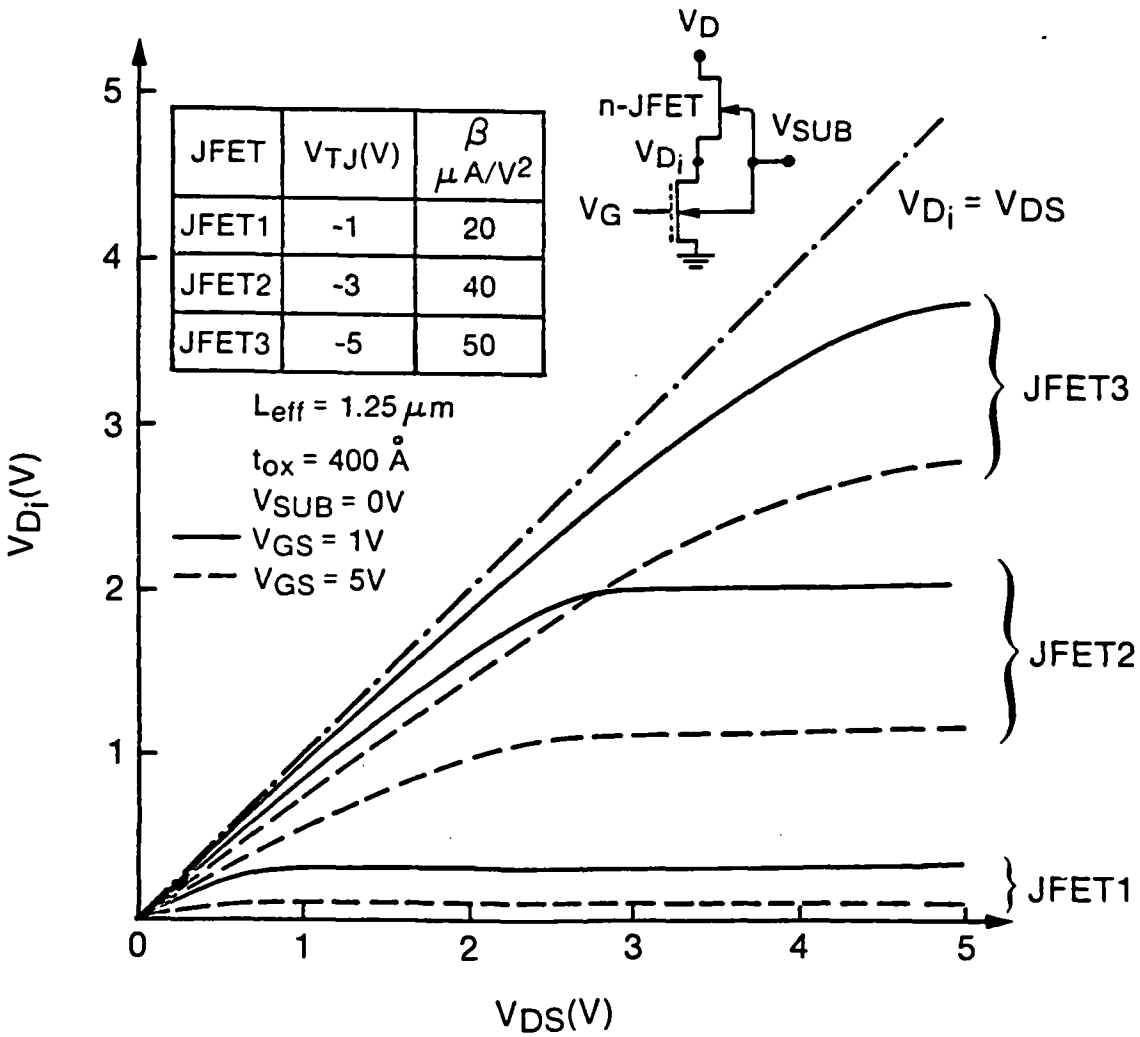

Fig. 5. Voltage transfer function from the externally applied JMOSFET drain bias (V_{DS}) and the voltage at the intrinsic drain of the surface channel MOSFET (V_{D_i}) for three different JFET designs.

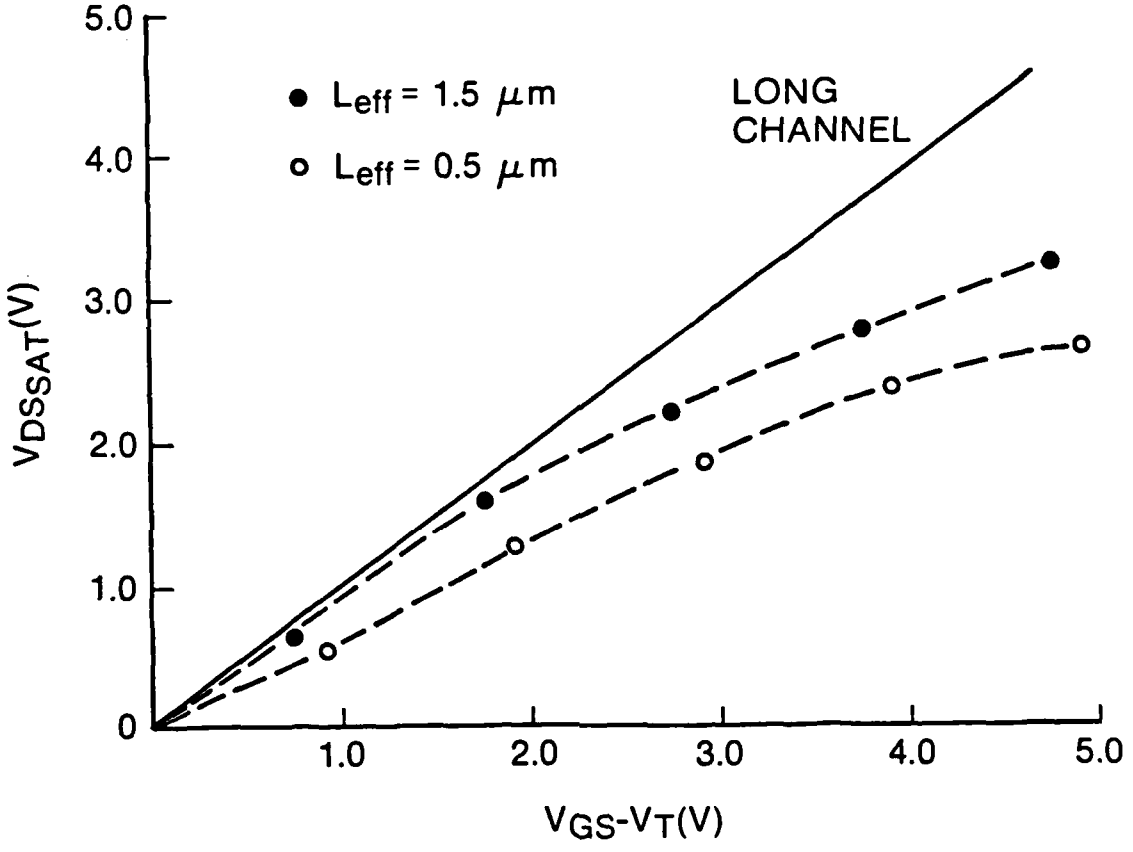

Fig. 6. Saturation drain voltage dependence on $V_{GS} - V_T$ for a conventional n-channel MOSFET.

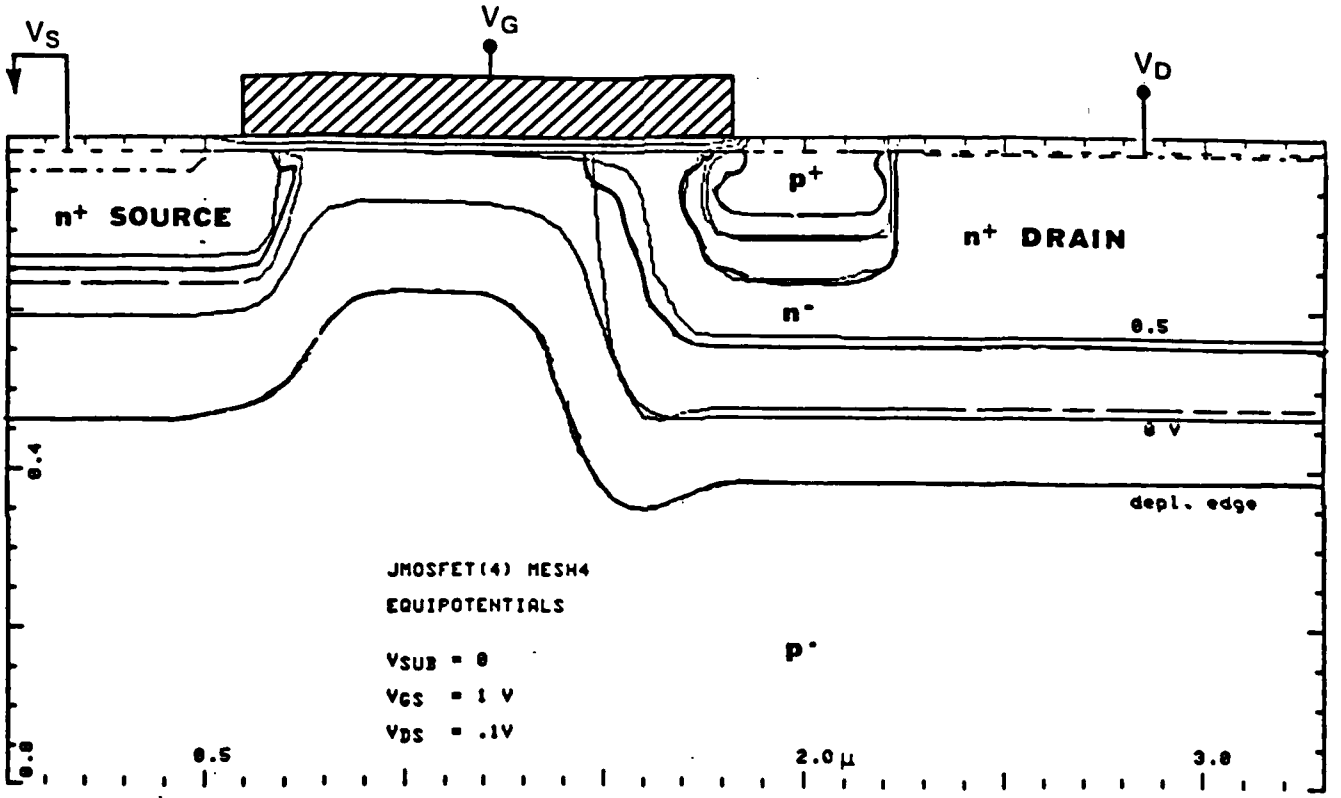

Fig. 7. PISCES simulated equipotential contours for the JMOSFET with $L_{eff} = 0.72\mu m$, $t_{ox} = 200\,\text{Å}$, $V_{T_J} = -1.6\,\text{V}$, V_{SUB}=0 V. Linear region bias of JFET. V_{DS}=0.1 V V_{GS}=1 V.

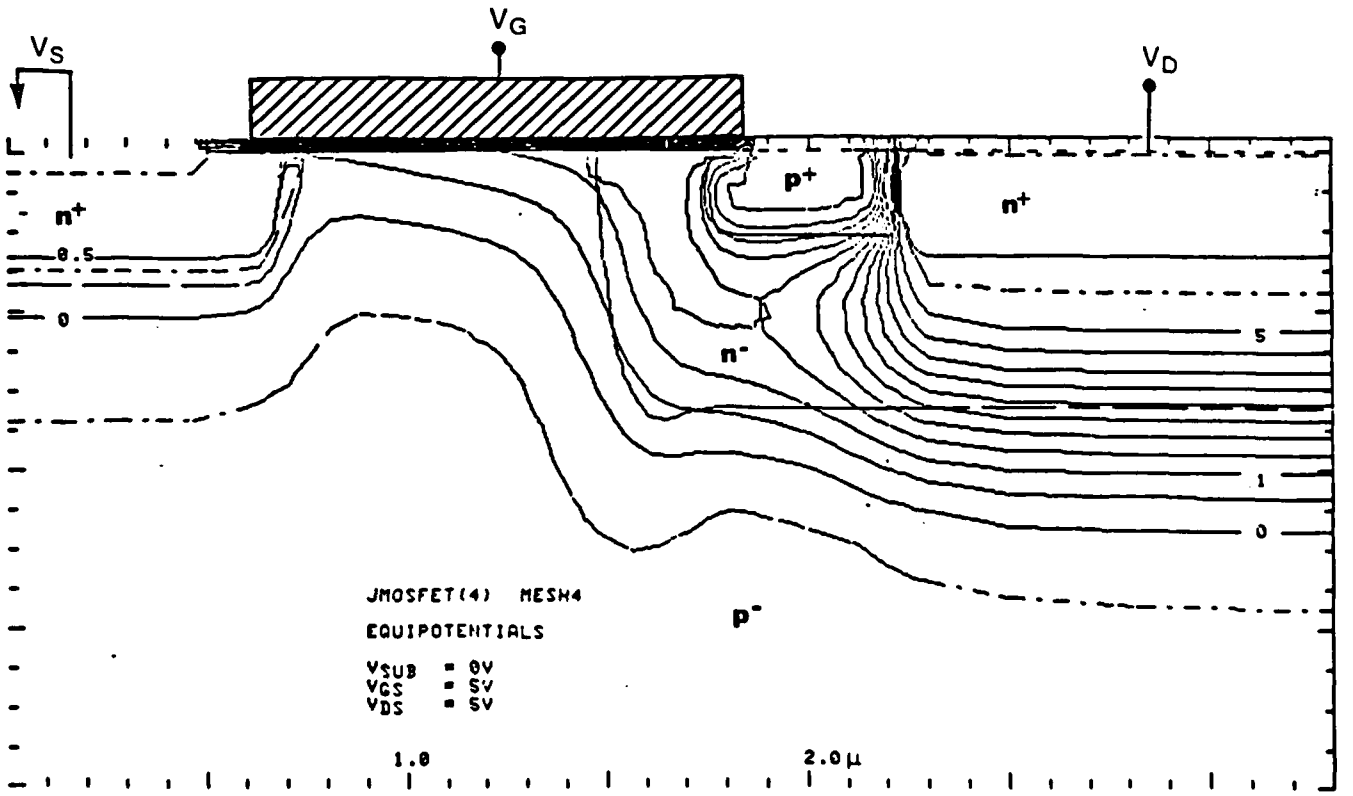

Fig. 8. PISCES simulated equipotential contours for the JMOSFET of Fig.7. JFET is pinched off at V_{DS}=V_{GS}=5 V.

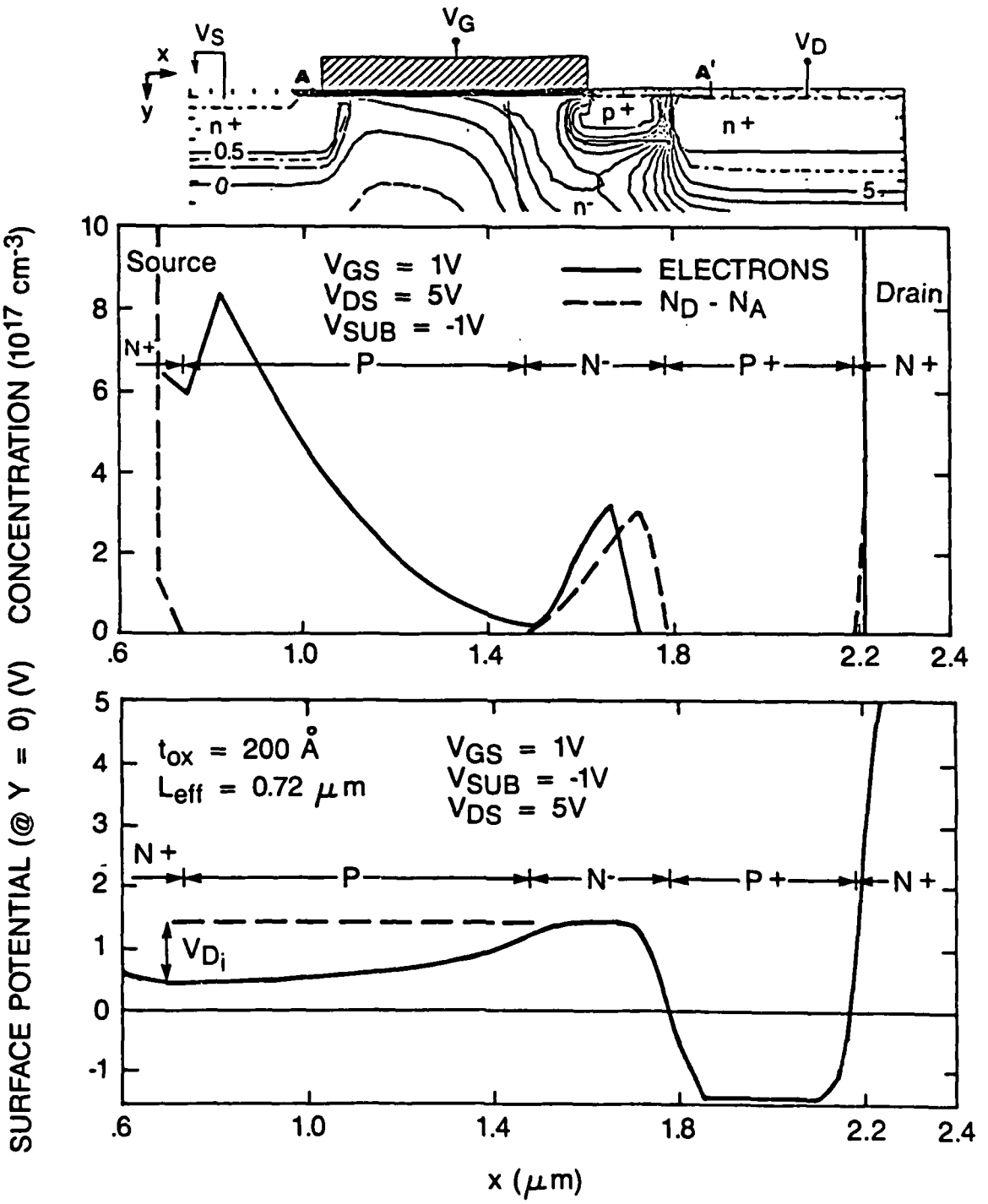

Fig. 9. PISCES simulated variation of: a) Electron and (input-specified) Net Donor densities; b) Potential along Si/SiO2 interface (line $A - A'$). JMOS structure of Fig.7. $V_{SUB} = -1$ V, $V_{DS} = 5$ V, $V_{GS} = 1$ V.

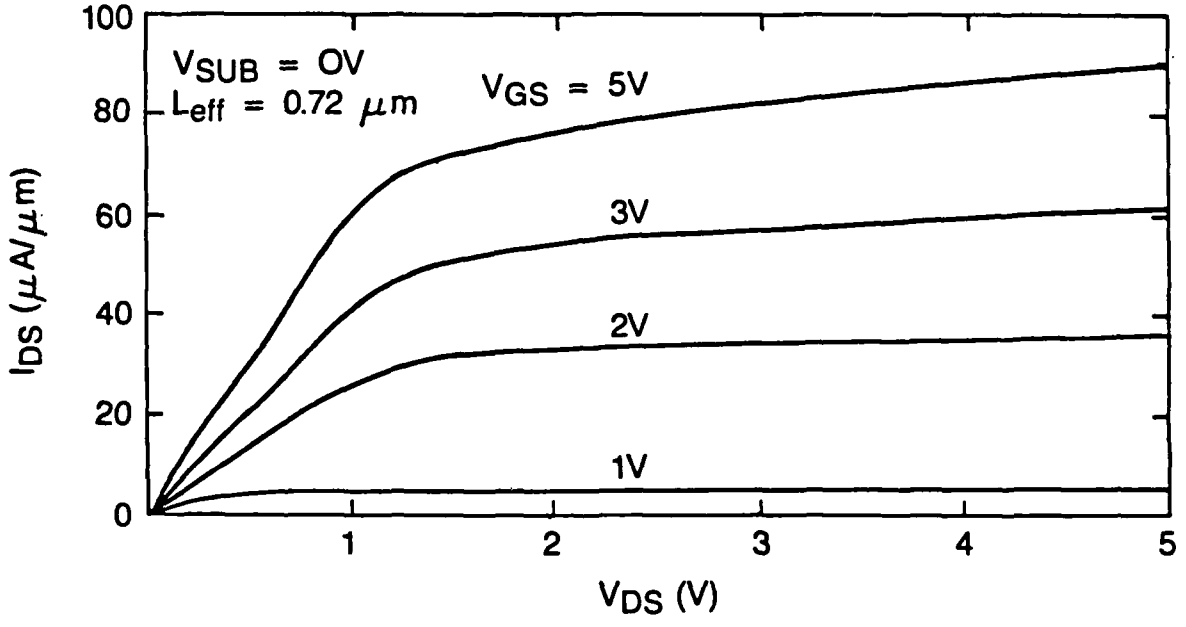

Fig. 10. PISCES simulated $I_{DS} - V_{DS}$ for $V_{T_J} = -1.6\,\text{V}$. JMOSFET structure of Fig.7. $V_{SUB} = 0\,\text{V}$.

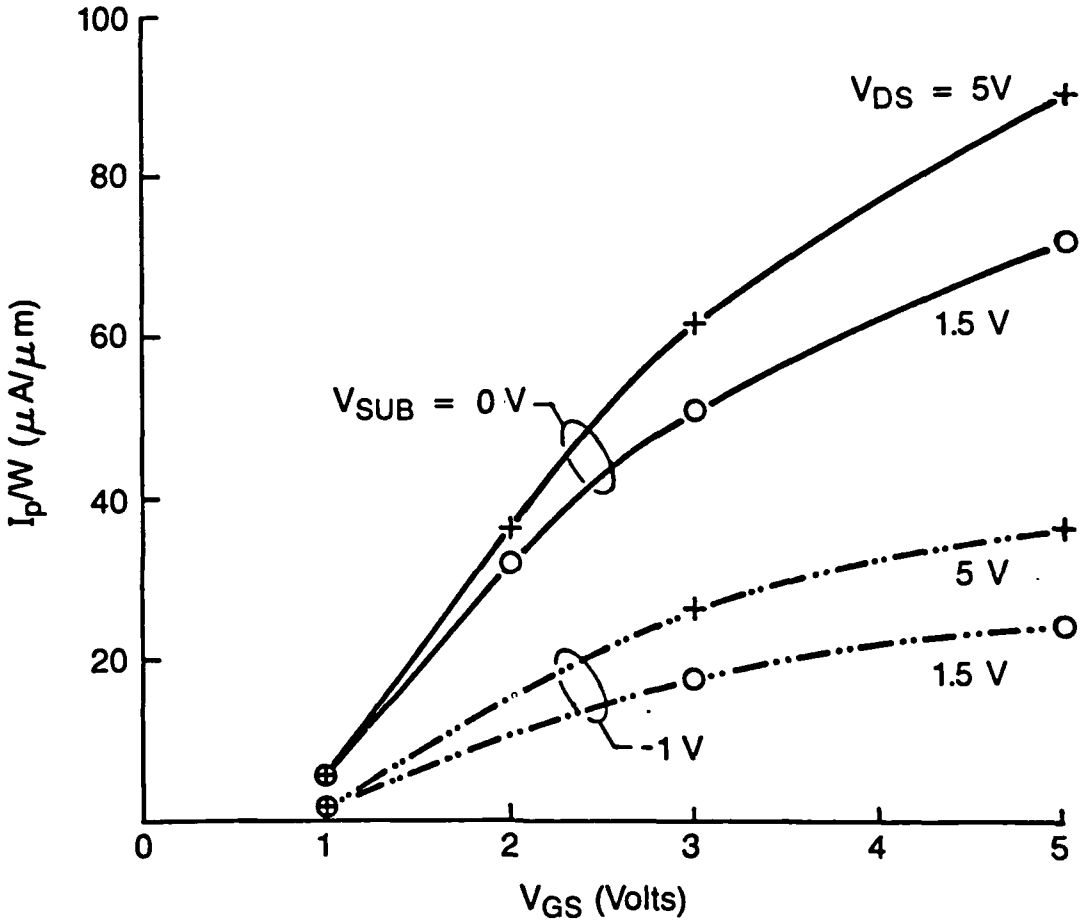

Fig. 11. Pinch-off current per unit channel width dependence on V_{GS}. PISCES simulated for the JMOSFET structure of Fig.7. $V_{SUB} = 0$ V.

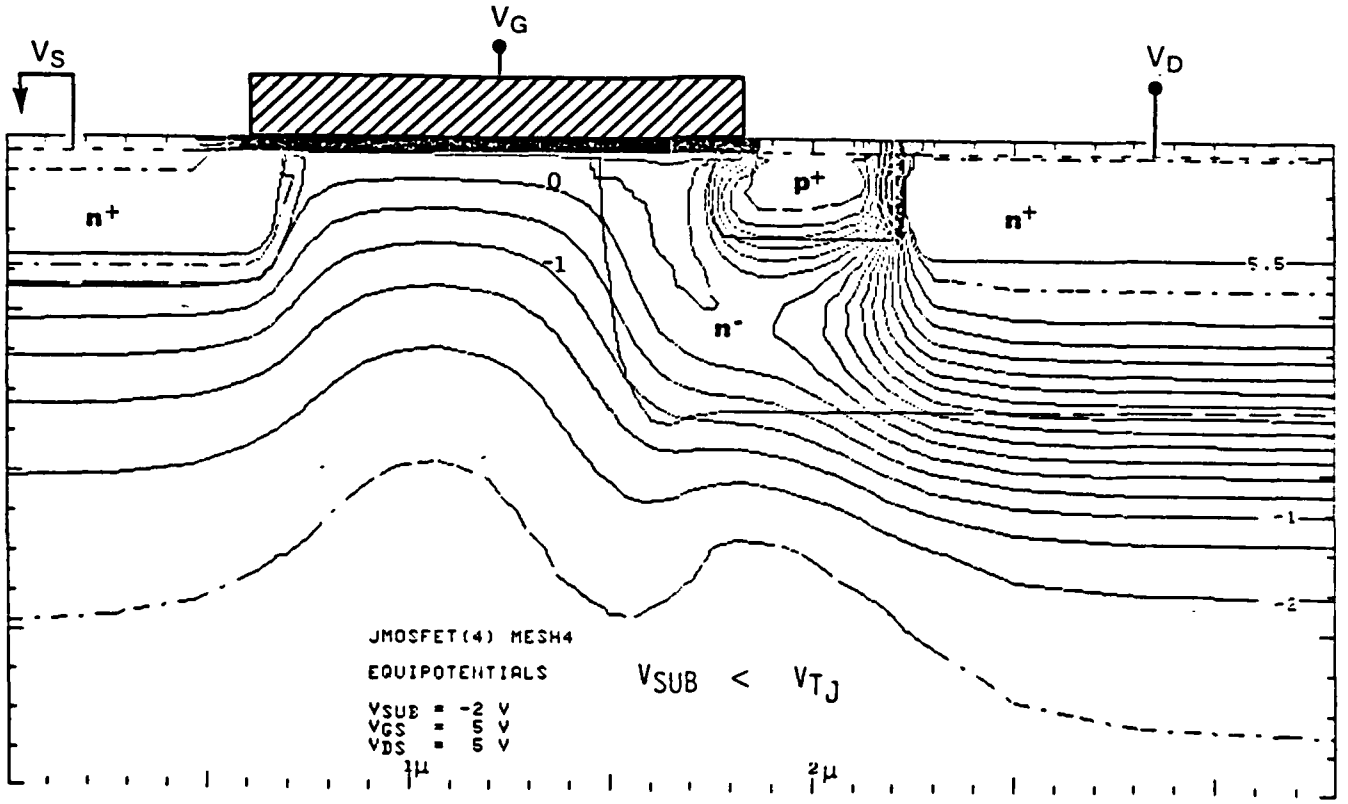

Fig. 12. Pisces simulated equipotential contours for the JMOSFET sctructure of Fig.7. V_{DS}=V_{GS}=5 V. MOSFET is ON and JFET is OFF at $V_{SUB} = -2$ V.

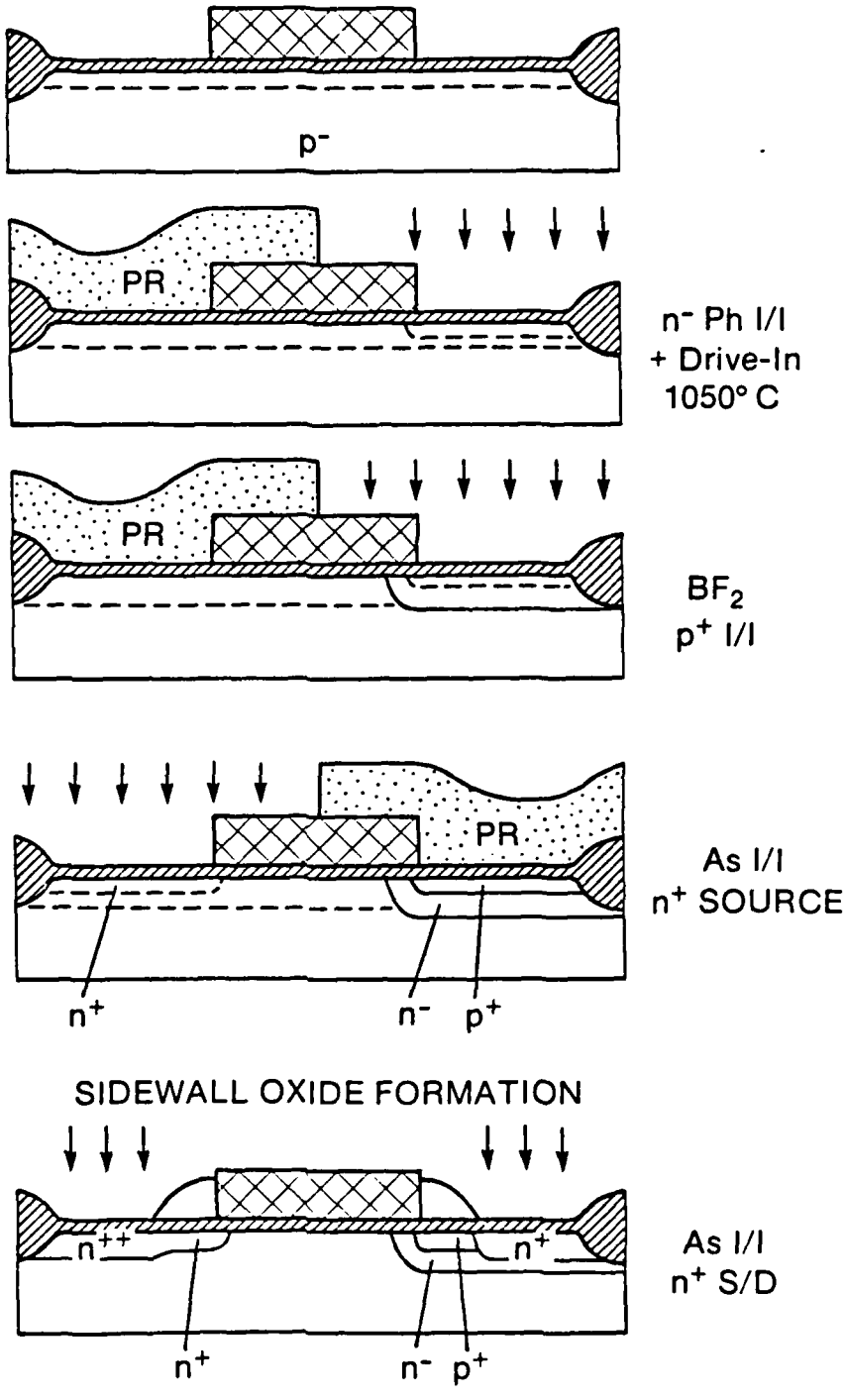

Fig. 13. Process sequence for JMOS fabrication.

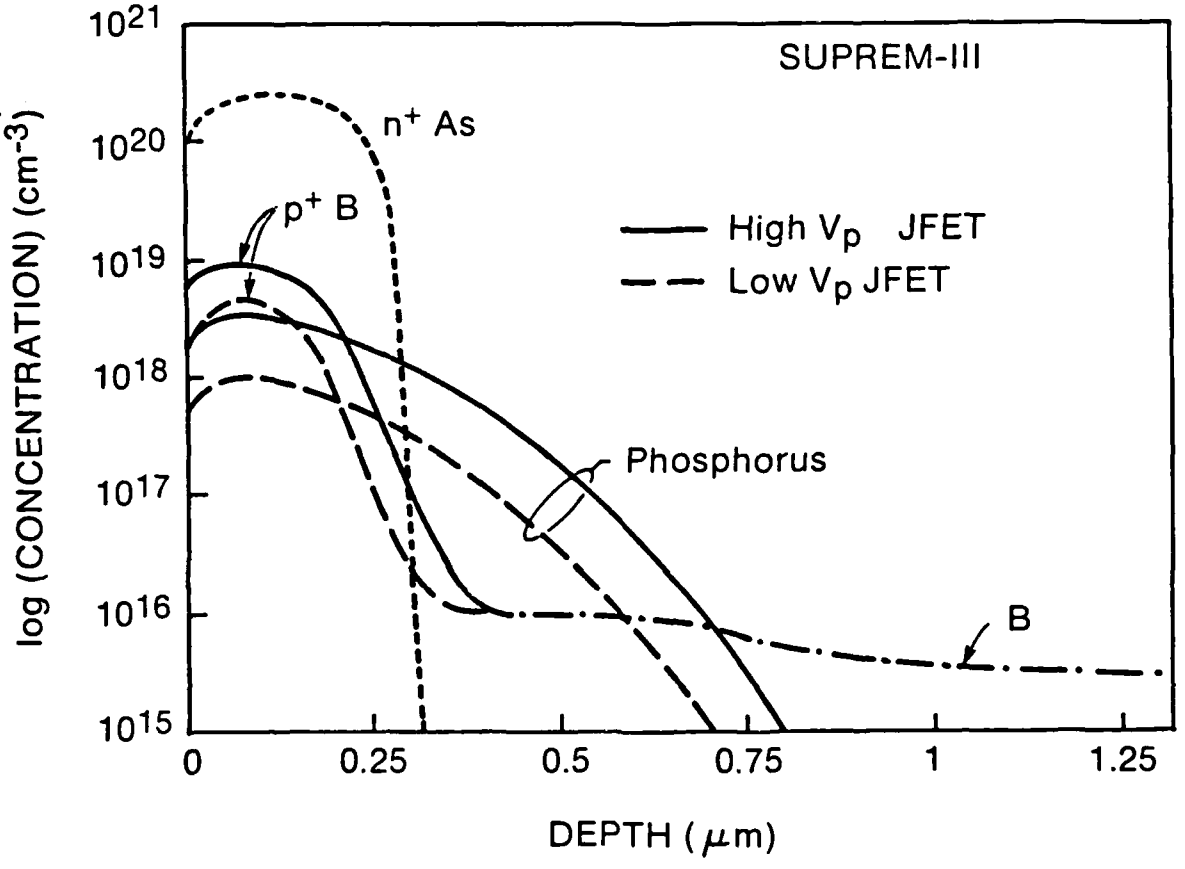

Fig. 14. SUPREM simulated impurity profiles for both JFET high-V_p and low-V_p designs.

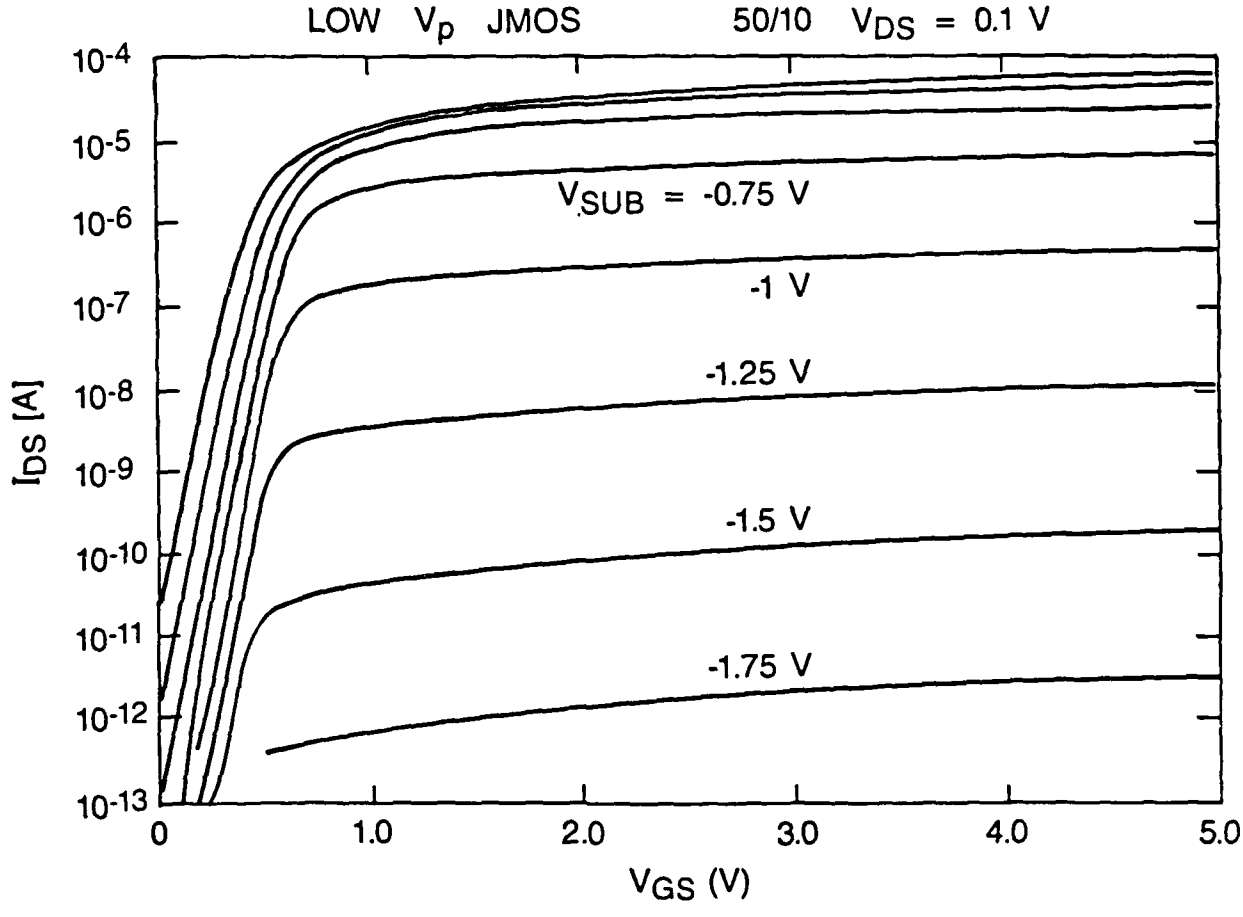

Fig. 15. Measured subthreshold characteristics for the low-V_p JMOSFET. $(W/L) = (50/10)$, V_{DS}=0.1 V , V_{SUB} steps $\Delta V_{SUB} = -0.25\,V$ from 0 to $-2\,V$.

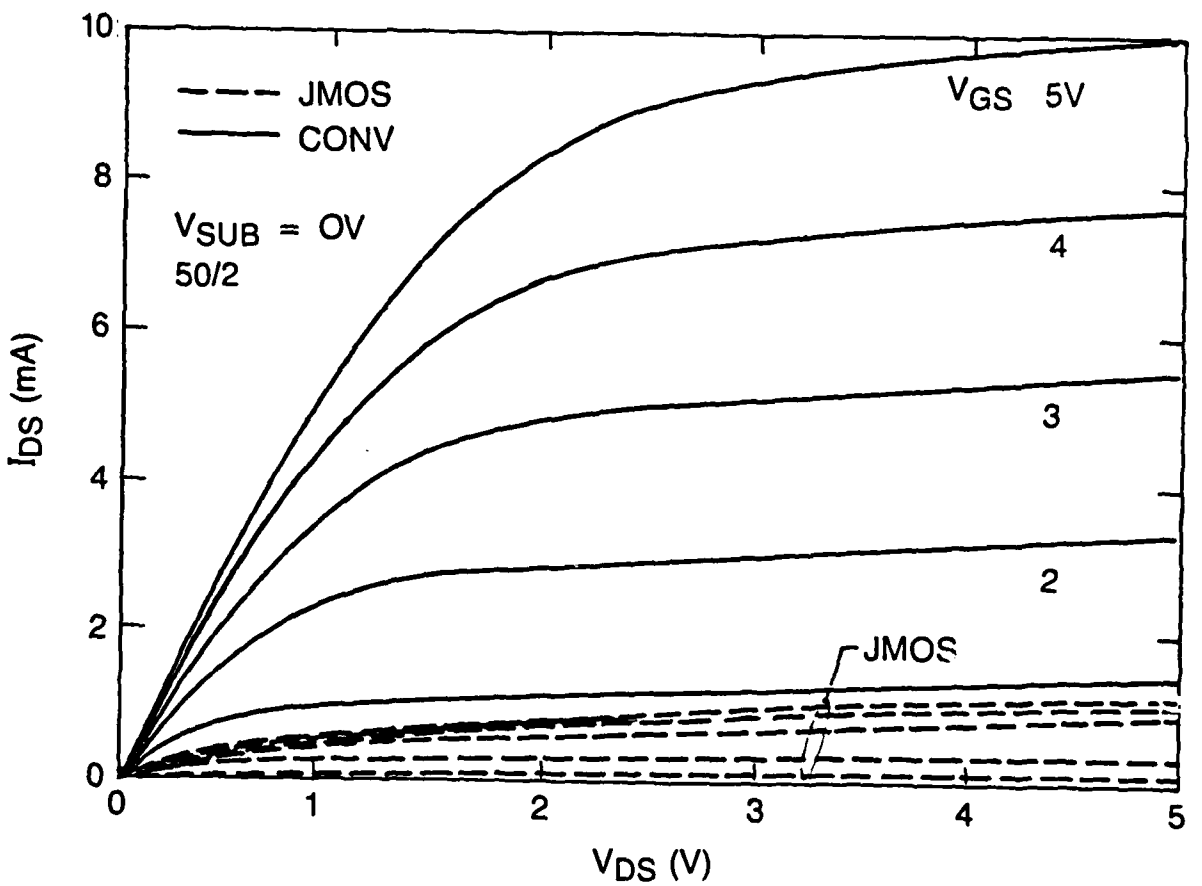

Fig. 16. Comparison of measured $I_{DS} - V_{DS}$ characteristics for the low-V_p JMOSFET and conventional device. Both devices have the same drawn $(W/L) = (50/2)$.

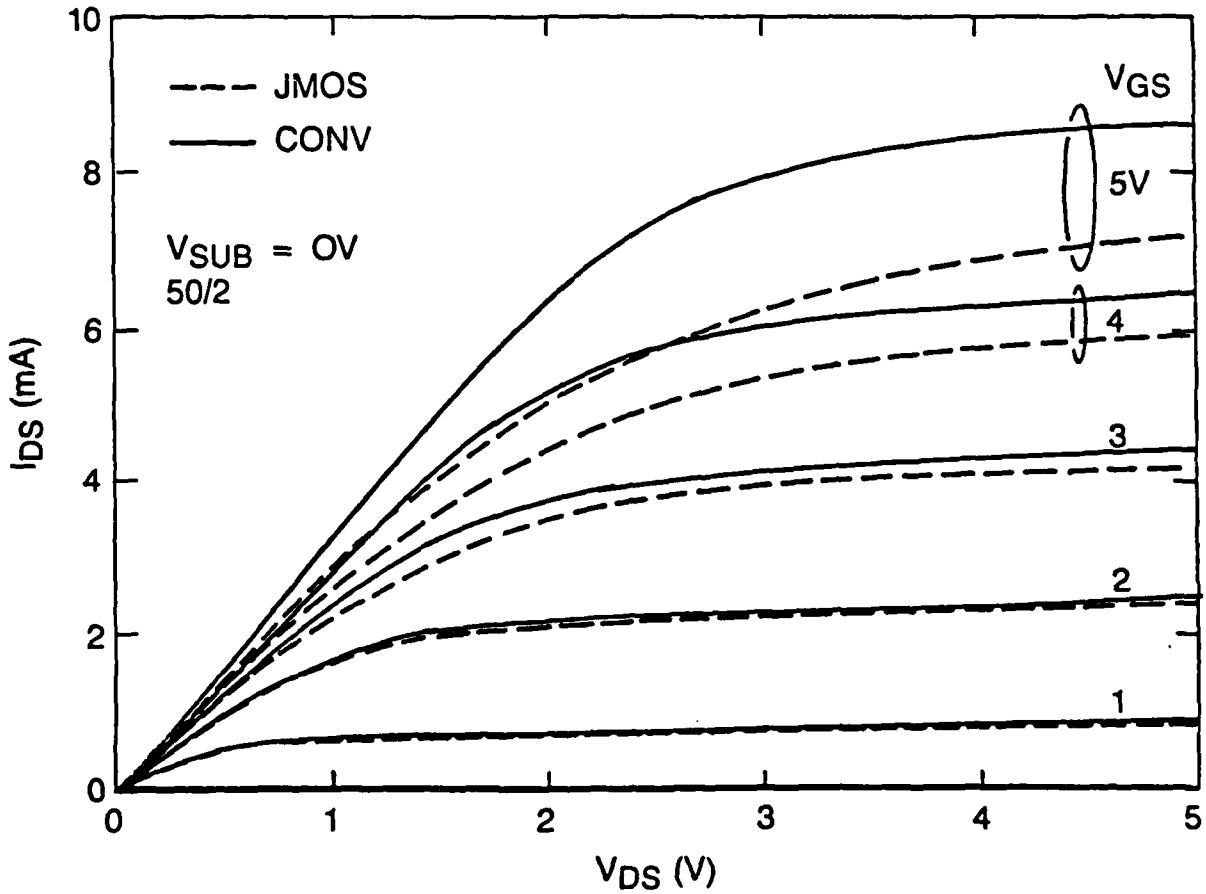

Fig. 17. Comparison of measured $I_{DS} - V_{DS}$ characteristics for a higher V_p JMOSFET and conventional device. Both devices have the same drawn $(W/L) = (50/2)$.

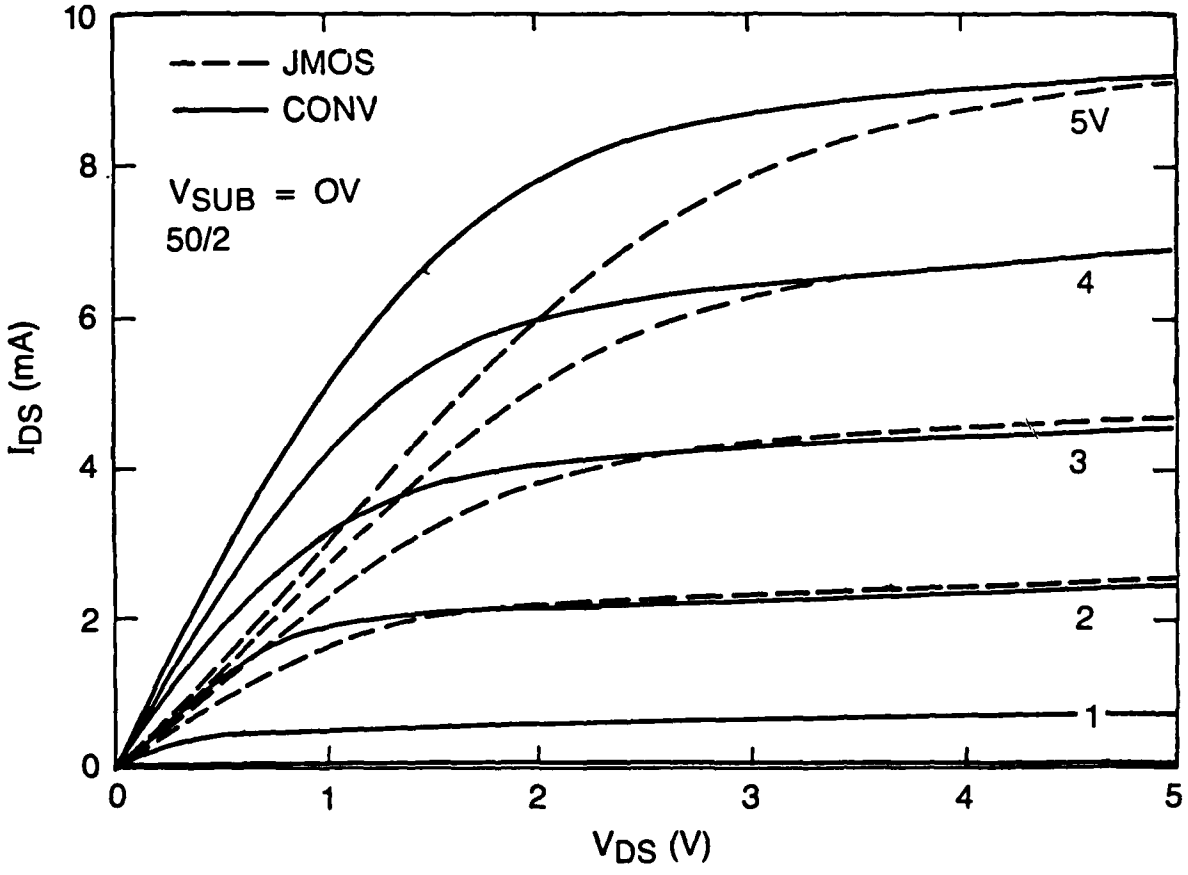

Fig. 18. Comparison of measured $I_{DS} - V_{DS}$ characteristics for the high-V_p JMOSFET and conventional device. Both devices have the same drawn $(W/L) = (50/2)$.

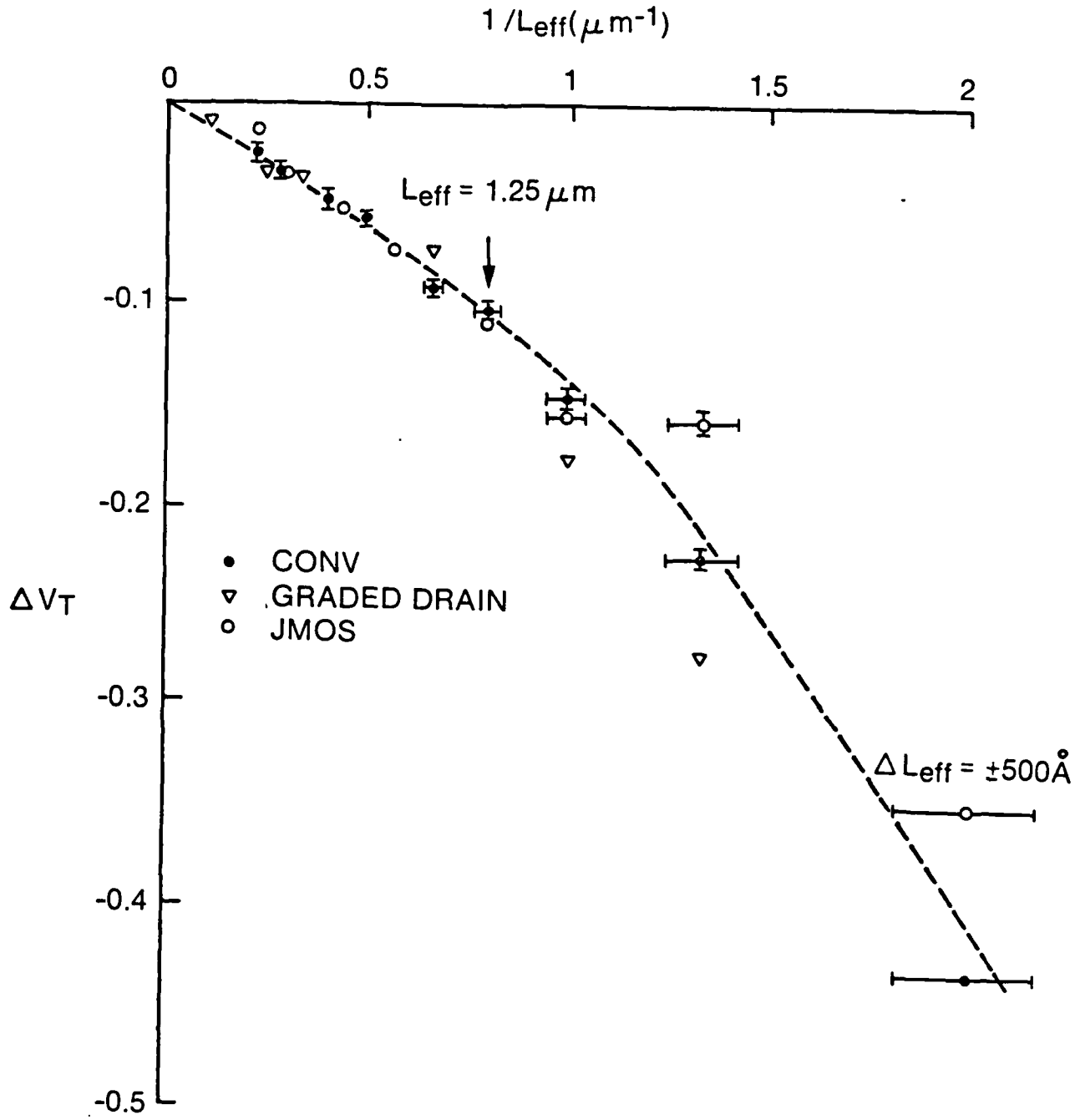

Fig. 19. Linear region threshold shift as a function of effective channel length. V_T extrapolation measurement at V_{DS}=100 mV.

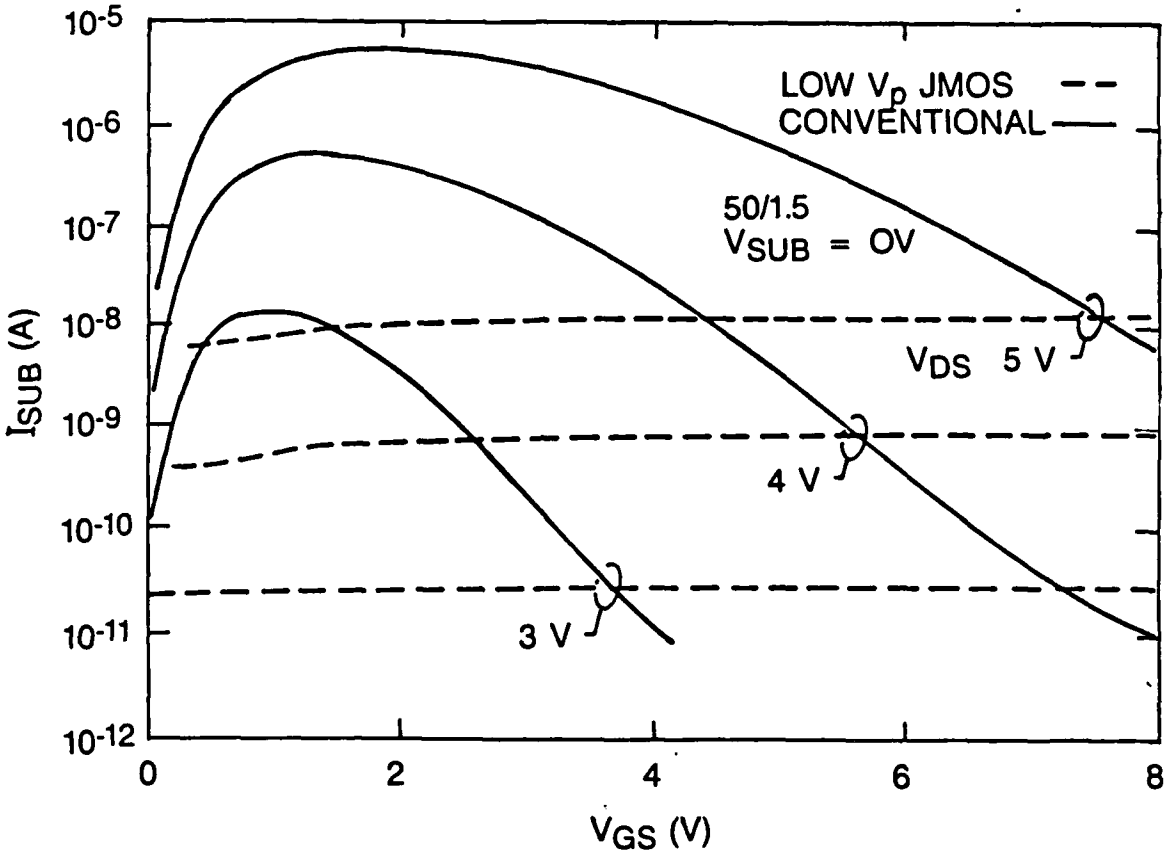

Fig. 20. Substrate current vs. V_{GS} comparison for conventional (solid line) and low-V_p JMOS (dashed) at V_{DS}=3,4,5 V. Drawn (W/L) = (50/1.5) for both devices. Low-V_p $L_{eff} = 0.8\mu m$, conv $L_{eff} = 1.0\mu m$.

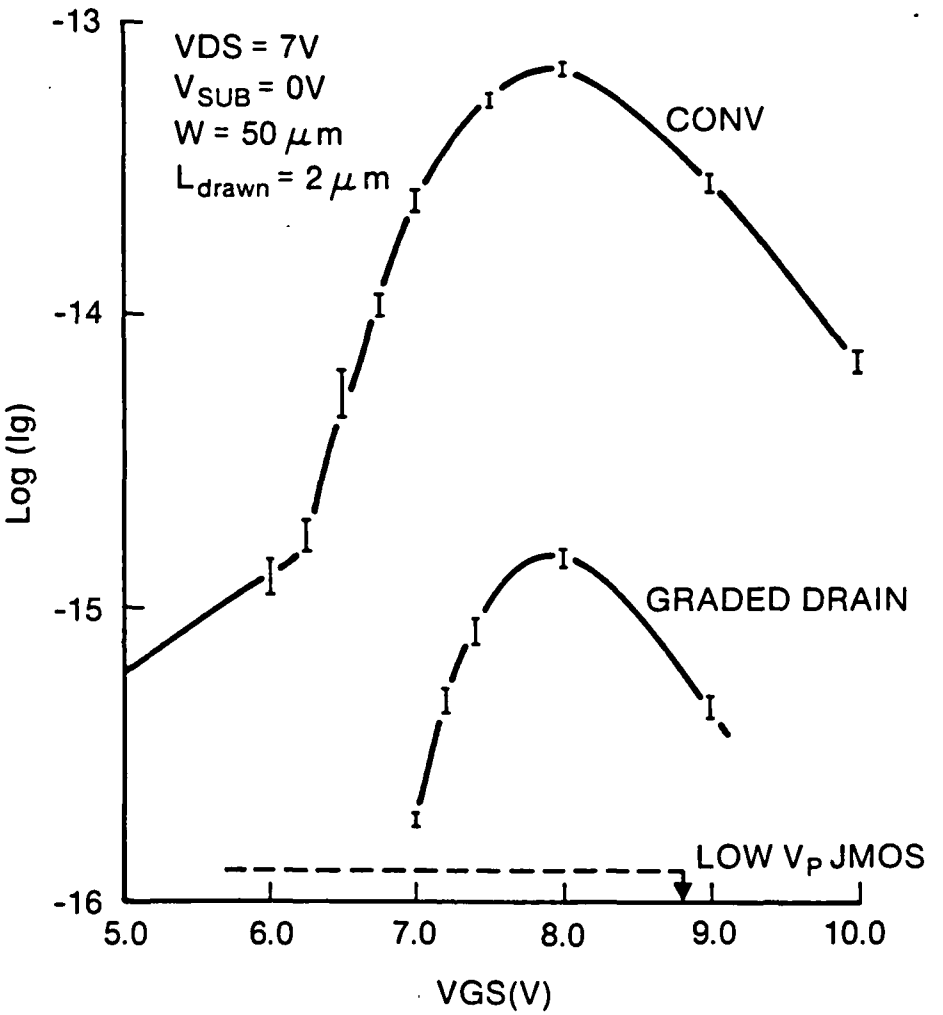

Fig. 21. Gate current vs. V_{GS} comparison for conventional and low-V_p devices. Both have drawn $(W/L) = (50/2)$. Conv. $L_{eff} = 1.5\mu m$, JMOS $L_{eff} = 1.3\mu m$. V_{DS}=7 V, $V_{SUB} = 0$ V. Graded S/D device with $L_{eff} = 1.1\mu$ is also shown.

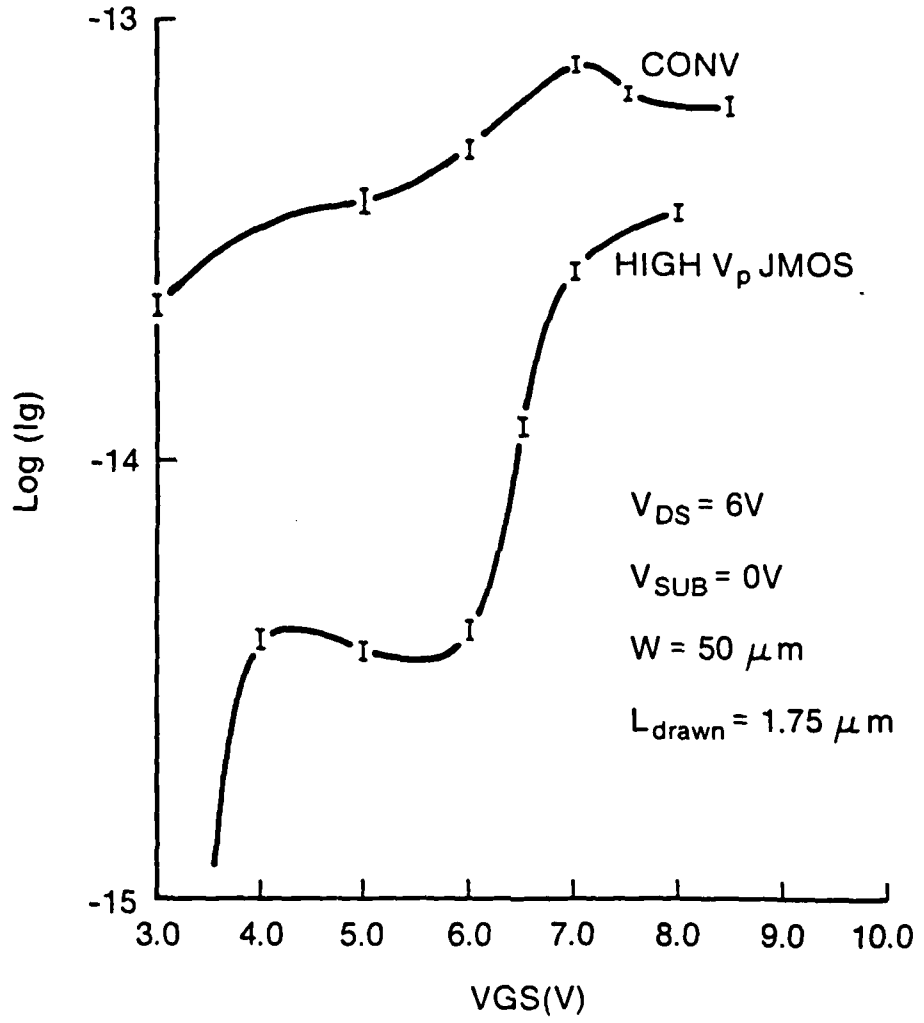

Fig. 22. Gate current vs. V_{GS} comparison for conventional and High-V_p devices. Both have drawn (W/L) = (50/1.75). Conv. L_{eff} = 1.2μm, JMOS L_{eff} = 1.0μm. V_{DS}=6 V, V_{SUB} = 0 V.

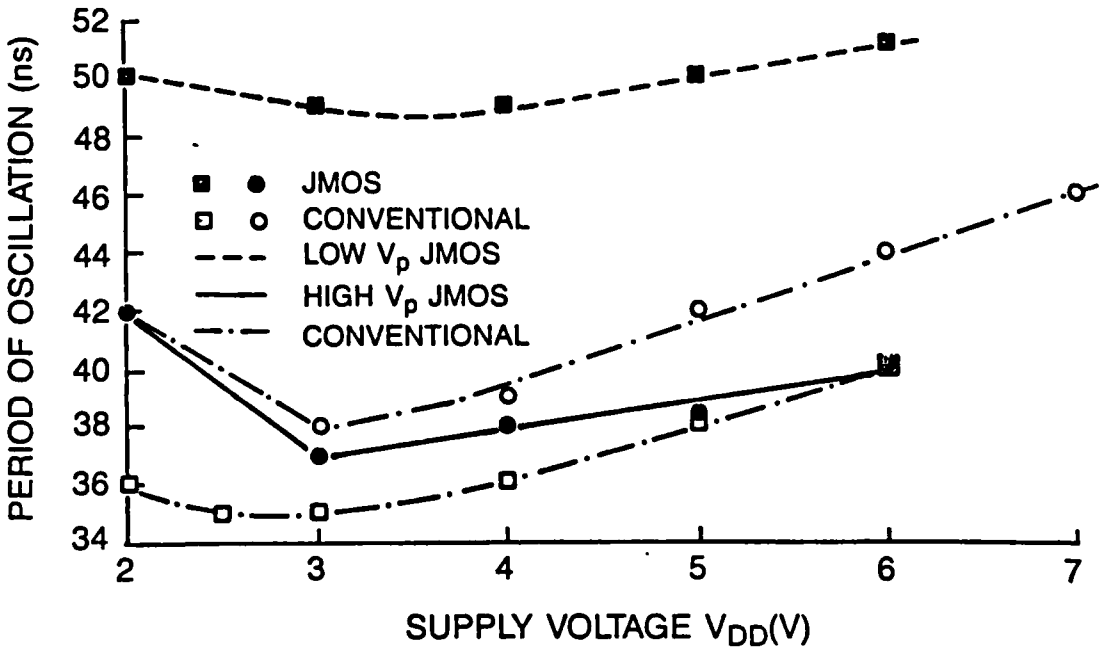

Fig. 23. E/D ring-oscillator period of oscillation vs. supply voltage. Boxes (□ ■) indicate the low-V_p experiment. Circles (○ ●) indicate the high-V_p experiment

END

DTIC

8-86